Key Features of Turing Systems are Determined Purely by Network Topology

Xavier Diego,[1,2,3,*] Luciano Marcon,[4,5] Patrick Müller,[4] and James Sharpe[1,2,6,3]

[1]*Center for Genomic Regulation, Barcelona Institute for Science and Technology, 08003 Barcelona, Spain*
[2]*Universitat Pompeu Fabra, 08003 Barcelona, Spain*
[3]*European Molecular Biology Laboratory, Barcelona Outstation, 08003 Barcelona, Spain*
[4]*Friedrich Miescher Laboratory of the Max Planck Society, 72076 Tübingen, Germany*
[5]*Centro Andaluz de Biología del Desarrollo, Consejo Superior de Investigaciones Científicas, Universidad Pablo de Olavide, 41013 Seville, Spain*
[6]*Institucio Catalana de Recerca i Estudis Avancats, 08010 Barcelona, Spain*

(Received 10 October 2017; revised manuscript received 23 March 2018; published 20 June 2018)

Turing's theory of pattern formation is a universal model for self-organization, applicable to many systems in physics, chemistry, and biology. Essential properties of a Turing system, such as the conditions for the existence of patterns and the mechanisms of pattern selection, are well understood in small networks. However, a general set of rules explaining how network topology determines fundamental system properties and constraints has not been found. Here we provide a first general theory of Turing network topology, which proves why three key features of a Turing system are directly determined by the topology: the type of restrictions that apply to the diffusion rates, the robustness of the system, and the phase relations of the molecular species.

DOI: 10.1103/PhysRevX.8.021071

Subject Areas: Biological Physics Complex Systems, Nonlinear Dynamics

I. INTRODUCTION

In 1952, Alan Turing proposed a theory of biological morphogenesis to explain the emergence of spatial organization in the embryo [1]. The influence of this ground-breaking theory has been phenomenal, as it has subsequently been invoked to explain patterning processes in chemical reactions [2], nonlinear optical systems [3], semiconductor nanostructures [4], galaxies [5], predator-prey models in ecology [6], vegetation patterns [7], cardiac arrhythmias [8], and even crime spots in cities [9]. Yet, especially in the field for which Turing developed his ideas —developmental biology—it still suffers from concerns about its validity, which arose early on in its history.

Turing's original model consisted of two molecular species that would diffuse through the embryonic tissue and chemically react with each other. He proved that, under certain conditions, such a simple reaction-diffusion system should be able to spontaneously create periodic patterns in space. The idea that a self-organized symmetry breaking of molecular concentrations would be driven by diffusion was counterintuitive, as diffusion normally has the effect of smoothing spatial heterogeneities and tends to generate uniform distributions.

Doubts about the relevance of Turing's theory were compounded by the lack of conclusive evidence of their existence in real-world examples for almost 40 years after he proposed it. Analysis of simple Turing systems suggested two main reasons why they may be hard to find in nature or to create artificially. Firstly, in its original form, a Turing system requires two species that diffuse at significantly different rates [10], whereas, in reality, many species that might conceivably form Turing patterns have very similar diffusion rates. Secondly, there appeared to be only extremely narrow ranges of the reaction parameters that would be compatible with a Turing pattern. Achieving a pattern would, therefore, require setting these parameters with unrealistic precision [11]. This property seemed to make Turing patterns an unlikely phenomenon and intrinsically unrobust.

A partial solution to these severe limitations has been found experimentally. The first experimental confirmation of the existence of Turing patterns, found in the chlorite–iodide–malonic acid (CIMA) chemical reaction [12,13], suggested a method to circumvent the diffusion constraints. In the CIMA reaction, a color indicator was included to act as a visual read-out of the chemical patterns produced. This indicator bound reversibly to one of the reactants and effectively slowed down its diffusion [2,14]. A refinement of this method [15,16] has been followed in the design of almost all new chemical systems producing Turing patterns

*xavier.diego@embl.es

[17] and inspired most of the theoretical efforts to relax the diffusion constraints [18,19].

Recent years have seen a shift in interest from chemical systems back to the biological problem for which Turing conceived the idea—embryo development. In this context, models of biological pattern formation that can bypass the diffusion constraints have also been proposed. Again, these models follow the design of the CIMA reaction, including immobile cell receptors as part of the network to play the role of the immobile color indicator [20–23]. This design, shown schematically in Fig. 1, is only a partial solution because the relaxation of the diffusion constraints is not complete and because it requires a very specific topological arrangement. Regarding the allegedly intrinsic lack of robustness of Turing systems, early studies observed that the volume of the parameter space varies greatly between different models [24,25], but little is known about what determines this property.

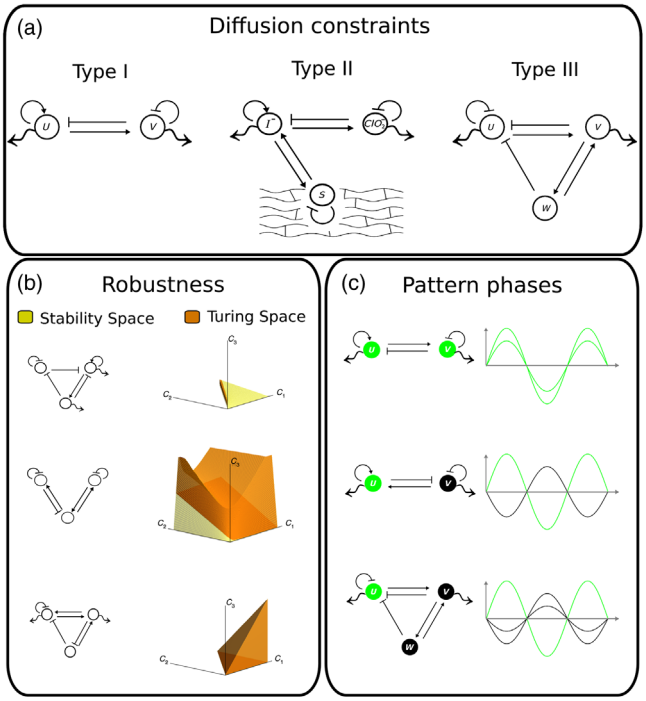

FIG. 1. Each panel illustrates a question about Turing systems that is resolved through analyzing the topology of the underlying network of interacting species. Namely, in a Turing system, how does the topology determine (a) the constraints on diffusion rates, (b) the size of the patterning parameter region, and (c) the phase of each species? More specifically, each panel contains three explicit networks with large differences in these properties. In all panels, edges ended with an arrow and a bar represent activation and inhibition, respectively. A wriggled arrow indicates that the node corresponds to a diffusible species. The two-species system illustrated in the left of (a) requires highly different diffusion rates of u and v for a pattern to exist, whereas the CIMA reaction schematic in the center can produce patterns with iodine (I^-) and chlorite (ClO_2^-) diffusing at the same rate. Finally, the network on the right produces patterns with no restriction on the diffusion rates. In (b), we see three three-species models whose Turing patterning parameter space are vastly different. The robustness of a patterning system can be assessed by the volume of the parameter sets compatible with reaction stability (shown in yellow) and diffusion-driven instabilities (shown in orange). For the three examples, the ratios of diffusion rates are the same, and the axes show the strength of the feedbacks between species. In (c), we present three networks and the prototypical patterns that they would produce in one dimension. The species whose concentrations are in phase are depicted in the same color.

However, a recent computational study showed that allowing more freedom to the interactions of the immobile species with the rest of the network could result in greater relaxation of the diffusion constraints [26]. This study showed that, in networks of three and four species, with only two diffusible species, it is possible to remove any constraints to their diffusion rates, a novel class of Turing networks that had not been found before. Further, the computational exploration showed that the percentage of networks with relaxed constraints was unexpectedly high. This finding requires a mechanistic explanation and suggests that central aspects of Turing networks have to be clarified.

Hence, we decided to investigate the relationship between the topology of a Turing network and its behavior using tools from graph theory. This proved to be fruitful, because we find that topology determines three fundamental properties of a Turing system illustrated in Fig. 1. Firstly, we demonstrate how the topology determines the diffusion constraints and the general method to relax or even remove them completely. Secondly, we are able show that Turing systems are not intrinsically unrobust because they do not require unphysical adjustment of parameters. Thirdly, our analysis allows us to resolve a question that, surprisingly, has not been addressed before: What determines the spatial overlap of the species in a Turing pattern? Again, we show that topology determines the spatial phases of the species and, further, that it is possible to construct a network with any desired pair of species overlapping in space.

In addition, our theory can be extended to oscillatory patterns and explains a new class of pseudopatterning networks that we call "Turing filters." The patterns generated by Turing filters do not have a characteristic wavelength; instead, these networks amplify preexisting spatial heterogeneities if their characteristic wavelength is smaller than a critical threshold, thus acting like a low-pass filter. Finally, we apply our theory to analyze experimental Turing systems, relevant models of biological pattern formation, and network designs proposed to genetically engineer Turing systems in cells.

Overall, these results show that our graph-based theory of Turing networks provides a unifying understanding of fundamental properties of these systems and constitutes a powerful aid to identify new self-organizing systems in nature or create them artificially.

II. GRAPH THEORY FOR TURING SYSTEMS

A system of interacting species whose concentration changes through local reactions and spatial diffusion can be described by a set of reaction-diffusion equations:

$$\frac{\partial r_i}{\partial t} = f_i(r) + d_i \nabla^2 r_i, \qquad i = 1, \ldots, N, \tag{1}$$

where $r_i(x,t)$, f_i, and $d_i \geq 0$ represent the concentrations, reaction rates, and non-negative diffusion constants. The homogeneous steady state is assumed to be stable, and there is no flow of reactants outside a finite domain. The existence of Turing patterns is demonstrated by analyzing the evolution of the system under small perturbations, which can be predicted from the linear approximation of the reaction-diffusion equations [27]. This leads to an eigenvalue problem that reduces the derivation of the conditions for diffusion-driven instability to the analysis of the zeroes of the characteristic polynomial $P_q(\lambda) = \det[\lambda \mathbf{I} - (\mathbf{J^R}(r_o) - q^2 \mathbf{D})]$, where $\mathbf{J^R}(r_0)$ is the Jacobian of the reaction term evaluated at equilibrium, and $\mathbf{D}$ is the diffusion matrix. The eigenvalues $\lambda(q)$ are given by the zeroes of $P_q(\lambda)$, and they determine the speed of growth or decay of the periodic mode of wavelength $2\pi/q$. The pattern that emerges is a superposition of the modes that grow, if there is any. For a system with N species, $P_q(\lambda)$ is a polynomial of degree N in λ:

$$P_q(\lambda) = \lambda^N + a_1(q)\lambda^{N-1} + \cdots + a_{N-1}(q)\lambda + a_N(q), \tag{2}$$

where the coefficients $a_k(q)$ are functions of the kinetic constants and the diffusion rates.

Thus, the conditions for diffusion-driven instabilities and whether they lead to stationary or oscillatory patterns can be obtained by analyzing the location of the zeroes of $P_q(\lambda)$ in the complex plane. In principle, this can be done analytically using the Routh-Huwitz theorem [28]. In practice, the conditions become intractable for networks with more than three diffusible species. Alternatively, graph theory provides tools that have been applied to the analysis of reaction network properties like stability [29,30], oscillations [31], and the detection of Turing bifurcations [32]. Building on this pioneering work, we introduce the reaction-diffusion graph to recast the algebraic Turing conditions in terms of the topology of the underlying reaction-diffusion system.

The reaction-diffusion graph is a directed graph of N nodes that follows closely the definition of the Coates graph of a square matrix [33]. Since every node corresponds to a species, these words will be used interchangeably. Intuitively, the reaction-diffusion graph reflects the interactions between the species in the system. Let f_{ij} denote the derivative of the reaction rate of the ith species with respect to the jth species evaluated at equilibrium. The reaction rates in Eq. (1) can be nonlinear functions (for example, if the reactions follow Michaelis-Menten kinetics), but the dynamics of the system near equilibrium can be determined from their linear approximation. If f_{ij} is not zero, it means that the jth species affects the reaction rate of the ith species, and there will be an edge from node j to node i with weight f_{ij}. According to this, if f_{ii} is not zero, it means that the reaction rate of the ith species has a decay or self-activation term, and we add an edge that starts and ends in the corresponding node. These edges are called "loops." The end of an edge reflects the sign of the interaction: an arrow for activation, a bar for inhibition, and a dot if it is unspecified. In addition, if a species is diffusible, we add a special type of loop represented by a wriggled arrow to the corresponding node. The weight of a diffusible loop is $-q^2 d_i$. This defines the reaction-diffusion graph that can be associated to any reaction-diffusion system. A detailed example of how to derive it from the reaction Jacobian is given in Appendix A.

Next, we show how the reaction-diffusion graph can be used to calculate the coefficients $a_k(q)$ in $P_q(\lambda)$. To that end, three basic graph-theoretical definitions are required: (i) A cycle is a closed path of k edges that joins k different nodes. It is said to be of length k, and its weight is simply the product of its edges. (ii) A linear spanning subgraph of k nodes (or ℓ-subgraph, for short) is a set of disjoint cycles that span them. It is said to be of size k, and its weight is the product of the weights of its cycles and a factor (-1) for each cycle. (iii) An induced subgraph is a subgraph formed by k different nodes and all the edges between them, and it is said to be of size k. Its complementary subgraph is the subgraph induced by the $N-k$ nodes that do not form part of it (which will be denoted the complementary nodes). An induced subgraph may contain several ℓ-subgraphs and its weight is given by the sum of all of them. By these definitions, loops are cycles of length 1 and also ℓ-subgraphs of size 1 for the corresponding node. The weight of an ℓ-subgraph is positive if it is formed only by negative cycles or contains an even number of positive cycles. In this case, it is said to be a stabilizing ℓ-subgraph, whereas, if the weight is negative, it is destabilizing. Examples to illustrate the following definitions are given in Appendix A.

Importantly, the coefficient $a_k(q)$ of $P_q(\lambda)$ is given by the sum of all the ℓ-subgraphs of size k. This central result can be derived using the Laplace expansion of the characteristic polynomial [34] and the Coates-Harary formula for the determinant [35,36] [see the derivation of Eq. (A4) in Appendix A]. The calculation of the coefficients of $P_q(\lambda)$ is facilitated by the introduction of a symbolic notation for cycles. Intuitively, a loop at node i is represented by $\underset{i}{\textcircled{\scriptsize i}}$; a cycle of length 2 between nodes i and j is represented by $\underset{ij}{\downarrow\!\uparrow}$; a cycle of length 3 spanning nodes i, j, and k by $\underset{ijk}{\triangle}$; a cycle of length 4 spanning nodes $i, \ldots, l$ by $\underset{i\ldots l}{\square}$; and so on. A diffusive loop at the ith node is

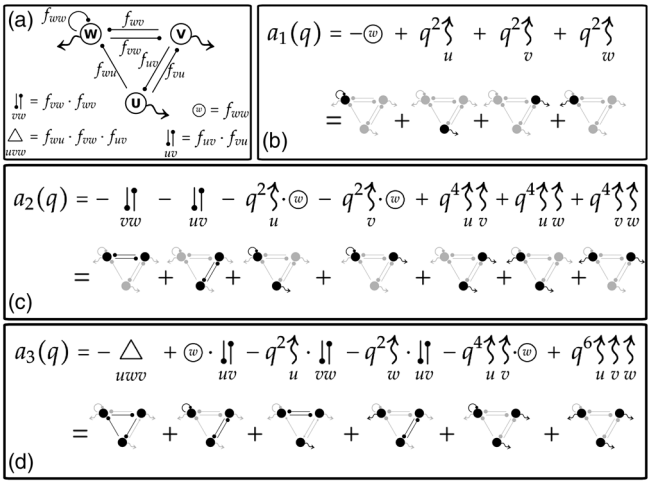

FIG. 2. (a) The reaction-diffusion graph of a three-species Turing system. Every edge is a nonzero entry of the reaction Jacobian, represented by f_{ij}. Wriggled arrows denote that the species is diffusible. Symbolic notation for its four reaction cycles is shown below: a loop at w; cycles of length 2 between u and v and between v and w; and a cycle of length 3 between u, w, and v. (b)–(d) Calculation of $a_k(q)$ for $k = 1, 2, 3$, given by the sum of all ℓ-subgraphs of size 1,2,3, respectively. Every contribution is shown in the upper row using a symbolic graph notation, with the corresponding ℓ-subgraph highlighted in black immediately below.

represented by $-q^{2}\updownarrow_{i}$. The calculation of $a_k(q)$ for a three-node topology is shown in Fig. 2 and more in detail in Appendix B for a four-node topology.

The coefficients $a_k(q)$ are then polynomials in q made of three types of contributions: (1) subgraphs formed only by reaction cycles, that will be referred to as ℓ_R-subgraphs, and form the independent term $a_k(0)$; (2) mixed subgraphs formed by (less than k) diffusive loops and nonoverlapping reaction cycles, which will be referred to as ℓ_{RD}-subgraphs and form the terms of degree smaller than q^{2k} in $a_k(q)$; (3) purely diffusive subgraphs, formed by combinations of k different diffusive loops, that form the terms of degree q^{2k} in $a_k(q)$.

The coefficients of $P_q(\lambda)$ are important because simplified conditions for diffusion-driven instabilities can be obtained in terms of their signs. The Routh-Hurwitz theorem, conversely, is general but even for moderately sized networks provides very little analytical insight [28]. A comprehensive discussion of the derivation and scope of the following simplified conditions is given in Sec. I of the Supplemental Material [37].

A Turing system must be stable without diffusion, which requires all the coefficients $a_k(q)$ to be positive for $q = 0$. Hence, $a_k(0) > 0$ for $k = 1, \ldots, N$ is a necessary condition for stability and, conversely, $a_k(q) < 0$ for some k is a sufficient condition for diffusion-driven instabilities. Necessary conditions for the emergence of stationary Turing patterns can be derived in terms of the sign of $a_N(q)$:

$$\exists q > 0, \quad \forall\ k < N \Big|^{a_k(q)>0}_{a_N(q)<0} \Leftarrow \text{stationary}. \tag{3}$$

For oscillatory patterns, a similar condition can be derived in terms of $a_{k<N}(q)$, but it is generally only sufficient [31,38]:

$$\exists q > 0, \quad \exists k < N \Big|^{a_k(q)<0}_{a_N(q)>0} \Rightarrow \text{oscillatory}. \tag{4}$$

Two important results follow from the previous developments. First, the topology of a reaction-diffusion system, understood as the distribution of cycles and diffusion loops, determines exclusively the requirements for the existence of Turing patterns, since the coefficients $a_k(q)$ are functions of ℓ-subgraphs only. Therefore, the existence of Turing patterns imposes constraints on the relative weights of cycles, rather than individual kinetic parameters. Second, a Turing system must have a destabilizing module, i.e., an induced subgraph in which the destabilizing ℓ_R-subgraphs outweigh the stabilizing ℓ_R-subgraphs. Typically, this condition requires a set of nodes linked by a positive cycle (highlighted in red in the rest of the text) that outweighs any other stabilizing ℓ_R-subgraphs contained in their induced subgraph. If a network does not a have destabilizing module, $a_k(q)$ are monotonically increasing functions of q, and the Turing conditions cannot be met. This is true for all Turing systems, except a small set of oscillatory networks that do not have a positive cycle. This constitutes the generalization of the requirement of a self-activator in two-node Turing networks. A rigorous proof of these results is given in Sec. II of the Supplemental Material [37]. Next, we use this graph-based framework to reveal the connection between the topology of a reaction-diffusion system and diffusion constraints, robustness, and pattern phases.

III. TOPOLOGY AND THE SOURCE OF DIFFUSION CONSTRAINTS

In a previous work, we developed a computational procedure to obtain an exhaustive list of three- and four-node networks with the minimal number of edges that can generate stationary Turing patterns [26]. The analysis revealed that three-node and four-node networks with two diffusible nodes could be classified into three types according to the diffusion constraints for the generation of Turing patterns. Defining the ratio of the diffusion rate of the diffusible species outside the destabilizing module to the diffusion rate of the species in it as d, and p as the space of kinetic parameters compatible with Turing patterns, the constraints for each type can be stated as

$$\begin{aligned} &\text{Type I}: \forall p,\ d > 1 \\ &\text{Type II}: \exists p,\ d = 1 \\ &\text{Type III}: \forall p,\ d > 0. \end{aligned} \tag{5}$$

Surprisingly, we found that there are as many three-node networks with one immobile reactant of type II and type III

as of type I, whereas the four-node networks with two immobile reactants of type III outnumber the networks of type I and type II. In other words, against the widely held belief, Turing networks with mild or no diffusion constraints are very common. Here, we demonstrate how the topology of a network explains these results and prove that the classification can be extended to general networks, regardless of the network size or the number of diffusible species.

According to the condition for Turing instability, $a_N(q)$ must cross zero and become negative for some $q > 0$. Decartes's rule of signs provides an upper bound for the number of real positive zeros of a real polynomial [39]. Particularly, a polynomial with only non-negative coefficients cannot have real positive zeros. All the independent terms $a_k(0)$ must be positive, according to the stability condition. The purely diffusive terms of $a_k(q)$, if present, are also strictly positive for $q > 0$. It then follows that $a_N(q)$ must have a negative coefficient, and the negative coefficient must lie at some intermediate degree in q^2. This is a necessary condition for stationary Turing instabilities.

In a network in which all the species diffuse, this is only possible with differential diffusivity. An algebraic proof of this well-known result is given in Sec. VI of the Supplemental Material [37], but it does not reveal the source of the requirement and how it can be weakened. To that end, it is necessary to examine the topology of the network.

The coefficient of degree $2m$ in $a_N(q)$, as shown in Eq. (A4), is the sum of all mixed ℓ_{RD}-subgraphs formed by m diffusive loops and an ℓ_R-subgraph that spans the other $N-m$ nodes of the network. Importantly, each of these ℓ_R-subgraphs of size $N-m$ contributes also to the coefficient $a_{N-m}(0)$ of $a_{N-m}(q)$. For example, in the topology shown in Fig. 2 the coefficient $a_3(q)$ is

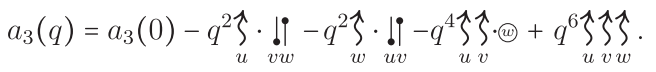

(6)

Thus, the coefficient of degree q^2 in $a_3(q)$ contains $\underset{vw}{\downarrow\uparrow}$ and $\underset{uv}{\downarrow\uparrow}$, which are all the ℓ_R-subgraphs that form the independent term $a_2(0)$ in $a_2(q)$. Likewise, the coefficient of degree q^4 in $a_3(q)$ contains $\circlearrowleft_w$, which is the only loop forming $a_1(0)$ in $a_1(q)$. This gives $P_q(\lambda)$ its nested structure:

(7)

Since stability imposes that $a_k(0) > 0$, the stabilizing subgraphs must outweigh the destabilizing subgraphs of size k. It follows that, for any of the coefficients of intermediate degree in $a_N(q)$ to be negative, the diffusion loops complementary to the destabilizing ℓ_R-subgraphs have to compensate for this difference. Thus, the differential diffusion requirement for Turing instabilities stems from Decartes's rule of signs. To illustrate the relationship explicitly in the network from Fig. 2, let the induced subgraph of u and v be the destabilizing module, and the cycle of length 2 between them the only positive cycle. Then, only the coefficient of degree q^2 in $a_3(q)$ can be negative. Imposing this and assuming for simplicity that the diffusion rates of the nodes in the destabilizing module (u and v) are equal, the constraint on the diffusion ratio $d = \uparrow_w / \uparrow_u = \uparrow_w / \uparrow_v$ takes the following form:

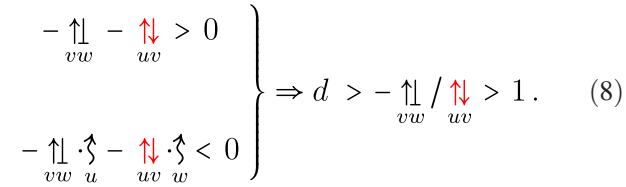

(8)

Two observations about the diffusion constraints are in order. First, the constraints on diffusion rates that stem from Decartes's rule are necessary for the existence of Turing patterns, but not sufficient. If the necessary ratio is set, the sufficient conditions are obtained, imposing that $a_N(q)$ turns negative, which results in additional requirements for the kinetic parameters but not for the diffusion rates. Second, the nested structure of the characteristic polynomial, combined with Decartes's rule, force that at least one species outside the destabilizing module has a larger diffusion rate than the species that induce it, and never the other way around. This is the generalization of the requirement of differential diffusion in two-node networks. In larger networks, the role of the activator and inhibitor cannot be assigned to individual species, but to network subgraphs. Importantly, the previous argument carries over for general networks of any size but depends on the assumption that all species diffuse. Each coefficient $a_k(0)$ is formed by all the reaction ℓ_R-subgraphs of size k. If all species diffuse, each ℓ_R-subgraph in $a_k(0)$ can be coupled to m diffusive loops of complementary nodes to form a mixed ℓ_{RD}-subgraph of size $k+m$ that contributes to the coefficient of degree $2m$ in $a_{k+m}(q)$. Thus, the nested structure of the characteristic polynomial, from which the diffusion constraints stem, is a general property of networks in which all species diffuse. Because of this, all networks in which all species diffuse belong to the type I class.

IV. RELAXATION OF DIFFUSION CONSTRAINTS

In networks with immobile species, the nested structure of the characteristic polynomial does not necessarily hold. This property is lost if there is at least one ℓ_R-subgraph with a complementary node that is immobile. Assuming that this subgraph is of size k, it will contribute to $a_k(0)$, but it will not contribute to $a_N(q)$. Particularly, it will be missing from

TABLE I. Topological features of Turing networks.

Type I	All stabilizing ℓ_R-subgraphs of the same size as the destabilizing module have all their complementary nodes diffusible.
Type II	At least one stabilizing ℓ_R-subgraph of the same size as the destabilizing module has an immobile complementary node.
Type III	The destabilizing module is the ℓ_R-subgraph of smallest size that has all its complementary nodes diffusible.

the coefficient of degree $2m$ in $a_N(q)$ formed by products of ℓ_R-subgraphs of size k and $m = N - k$ diffusion loops. If the missing subgraph is stabilizing and of the same size as the destabilizing module, the requirements on the diffusion rates stemming from Decartes's rule are weakened. The destabilizing module can outweigh the remaining subgraphs and make the coefficient of degree $2m$ in $a_N(q)$ negative, even if the diffusion loops of its complementary nodes are equal or smaller than its own. In this way, the necessary condition of differential diffusivity is weakened.

By the same mechanism, the stabilizing influence of subgraphs of smaller size than the destabilizing module might vanish. This would be reflected in the disappearance of terms of degree higher than $2m$ in $a_N(q)$, which in turn facilitates the fulfillment of the sufficient condition for the existence of Turing patterns.

This is the principle that underlies the relaxation of diffusion constraints and the associated classification of Turing networks. The precise topological characterization of each type of Turing system is given in Table I.

The different Turing types can also be distinguished easily by the algebraic form of the characteristic polynomial. In type III networks, the destabilizing module is the only contributor to the leading term in $a_N(q)$. Hence, for all modes with wave number q above a certain threshold, $a_N(q)$ turns negative and the system is unstable independently of the diffusion rates. Both the necessary condition derived from Decartes's rule and the sufficient condition $a_N(q) < 0$ are guaranteed by the topology. There are two configurations that result in a type II network. In the first configuration, the destabilizing module is the only contributor of its size to a coefficient in $a_N(q)$, but there are stabilizing subgraphs of smaller size that contribute to coefficients of higher degree. It follows that the necessary condition is guaranteed by the topology, but the sufficient condition still involves the diffusion rates. In the second configuration of type II networks, the destabilizing module is not the only contributor of its size to $a_N(q)$, but at least one stabilizing subgraph of the same size is missing. Thus, the necessary condition is not guaranteed by the topology, but it can be fulfilled without differential diffusion. Whether there are terms of higher degree or not determines if the sufficient condition is satisfied automatically or if it imposes additional requirements on the kinetic rates. In type I networks, all subgraphs of the same size as the destabilizing module contribute to $a_N(q)$. Hence, the necessary condition imposes differential diffusion. Again, if there are coefficients of higher degree, they further restrict the space of parameters compatible with Turing instability.

The principle for the relaxation of diffusion constraints is illustrated in Fig. 3. Setting one node at a time as immobile in the minimal topology of Fig. 2 results in a Turing network of each type according to the diffusion constraints. If the subgraph induced by u and v is the destabilizing module and v is assumed to be immobile, the network shown in Fig. 3(a) is obtained. Then, the coefficient $a_3(q)$ of Eq. (6) is reduced to

$$a_3(q) = a_3(0) - q^2 \overset{u}{\wr} \cdot \underset{vw}{\uparrow\downarrow} - q^2 \overset{w}{\wr} \cdot \underset{uv}{\uparrow\downarrow} . \tag{9}$$

Hence, the network is still a type I Turing system limited by the constraint given in Eq. (8). The diffusion rate of w must be bigger than that of u; otherwise, the coefficient of degree q^2 cannot be negative. If this occurs, the sufficient condition $a_3(q)$ is fulfilled automatically for sufficiently large wave numbers. Conversely, the same topology becomes the type II network shown in Fig. 3(b) if the subgraph induced by w and v is the destabilizing module, and w is assumed to be immobile. Then, the coefficient $a_3(q)$ is

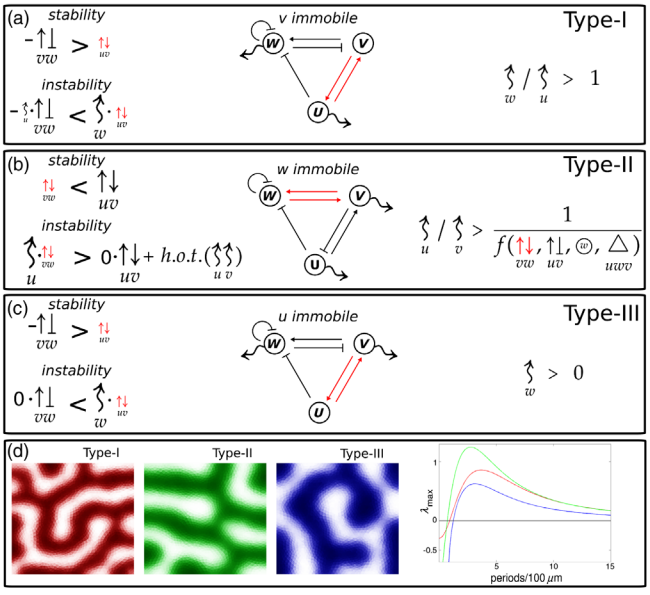

FIG. 3. (a)–(c) Permutation of the immobile node in the topology of Fig. 2 results in a Turing network of each type. In each panel, stability and instability requirements are shown on the left, with diffusion constraints on the right. (d) Patterns and dispersion relationships of type I, II, III are qualitatively similar.

$$a_3(q) = a_3(0) - q^2 \overset{\uparrow}{\underset{u}{\wr}} \cdot \underset{vw}{\updownarrow} - q^4 \overset{\uparrow}{\underset{u}{\wr}} \overset{\uparrow}{\underset{v}{\wr}} \cdot \textcircled{w} . \tag{10}$$

The destabilizing module is the only contributing term to the coefficient of degree 2 in $a_3(q)$, and the necessary condition that stems from Decartes's rule is fulfilled automatically and independently of the diffusion ratio d. Because there is a coefficient of larger degree in q, fulfillment of the sufficient condition $a_3(q) < 0$ involves the diffusion ratio, but as expected from a type II network, it can be satisfied with $d = 1$.

Finally, the topology of Fig. 2 is transformed into the type III network of Fig. 3(c), assuming that the subgraph induced by u and v is the destabilizing module and that u is not diffusible. In this case, the destabilizing module is the only contributor to the leading coefficient in $a_3(q)$:

$$a_3(q) = a_3(0) - q^2 \overset{\uparrow}{\underset{w}{\wr}} \cdot \underset{uv}{\updownarrow} . \tag{11}$$

Hence, the topology guarantees the fulfillment of both the necessary *and* the sufficient conditions for the existence of Turing patterns, independently of the diffusion rates.

The relaxation principle operating in the CIMA chemical reaction [2,15] and several models of biological patterning networks from the literature [19–21,23,40] are analyzed in Appendix D. The power of the graph-based framework to analyze more complex systems is illustrated in a four-node and even a ten-node network in Appendixes C and D; additional examples of nonminimal networks are analyzed in Sec. III of the Supplemental Material [37].

Understanding the topological mechanism that underlies the relaxation of diffusion constraints facilitates the design of Turing networks. Relaxation occurs if at least one stabilizing ℓ_R-subgraph of the same size as the destabilizing module has at least one complementary node that is immobile. The immobile node necessarily belongs to the destabilizing module, since its complementary nodes must all be diffusible. It follows that setting as immobile a node that is complementary to several stabilizing cycles is an efficient way to relax the diffusion constraints. Likewise, as more nodes of the destabilizing module are assumed to be immobile, it is more likely that subgraphs of the network lose their stabilizing influence and that the diffusion constraints are weakened. This is the reason why, in larger networks, which can have larger destabilizing modules that accommodate more immobile nodes, the fraction of type II and type III networks increases, as it was observed in Ref. [26] for networks of three and four nodes. In this way, the present theory explains this finding and predicts that this trend should increase for larger and more realistic networks.

V. TURING FILTERS AND OSCILLATORY TURING NETWORKS

The extreme case of Turing networks in which all nodes of the destabilizing module are immobile deserves special attention. We previously discovered that these networks are all type III [26]. Here, we demonstrate why their dynamic behavior is qualitatively different from standard Turing networks: The wavelength of the emergent pattern is not determined by the network, but by the external perturbation.

The reason is that the dispersion relationship does not have a peak that determines the pattern wavelength. Instead, the maximum eigenvalue grows monotonically from a negative value at $q = 0$ and tends asymptotically to a maximum positive value for large wave numbers. The proof of this result is given in Sec. IV of the Supplemental Material [37] using Rouche's theorem, and a network of this kind is shown in Fig. 4(a). Thus, modes with a wave number below the critical value are not amplified, whereas all the modes with a much larger wave number grow with comparable speeds. Therefore, the emergent patterns do not have a characteristic wavelength determined by the network. Instead, the initial perturbation that kicks the system out of the homogeneous equilibrium is what determines the pattern that emerges. If the initial perturbation has a spatial structure with a wavelength smaller than the critical value, the system amplifies it to form a stationary pattern with the same spatial structure. Conversely, an initial prepattern with wavelength above the critical value is not amplified. If the homogeneous state is driven out of equilibrium by a low amplitude white noise, all the modes present in the perturbation grow. In this scenario, the modes that grow faster are those with infinitely small wavelength and, for this reason, the system evolves to form a stationary salt-and-pepper pattern. In this sense, the type III networks in this subset are not genuine spontaneous pattern-forming systems, and they could rather be called Turing filters, since they behave as low-pass filters. Simulations showing the amplification of different prepatterns are shown in Fig. 4(a).

The results obtained so far have focused on stationary Turing patterns. However, the analysis can be extended to oscillatory Turing patterns with only minor modifications. Indeed, the classification according to diffusion constraints and the topological arrangements that distinguish the different types carries over for most networks generating oscillatory Turing patterns. These are the networks in which the instability occurs when a coefficient $a_{k<N}(q)$ turns negative, while $a_N(q)$ remains positive, like the network shown in Fig. 4(b). The subgraph that causes the instability spans $k < N$ nodes. An important difference is that the conditions for the existence of oscillatory Turing patterns are sufficient but not necessary. This means that not all networks capable of generating oscillatory Turing patterns are covered. The networks left out of the analysis are, however, rare and subject to severe constraints in their kinetic parameters. Interestingly, they can be built without any positive cycle and do not require differential diffusivity (see Sec. I of the Supplemental Material [37] for an expanded discussion). Oscillatory Turing filters also exist and like their stationary counterparts are characterized by having a destabilizing module composed of nondiffusible nodes. The design

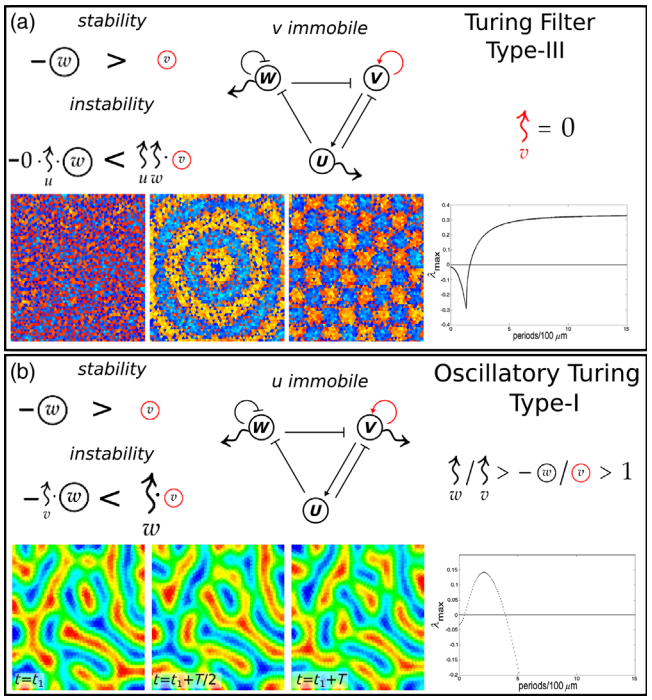

FIG. 4. Permutation of the immobile node in a three-node topology results in (a) a Turing filter because the destabilizing module is formed by a single immobile node. The simulations show the amplification of noisy, circular, and checkerboard initial conditions. The dispersion relationship, saturating at large wave numbers, determines the threshold for pattern amplification. (b) An oscillatory network of type I. The time points of the simulation show a spatially stationary and temporally oscillatory pattern. The real part of the eigenvalue (the dotted line in the dispersion relationship) determines the wavelength and the complex part (not shown) of the time period. In both panels, stability and instability requirements are shown on the left, with diffusion constraints on the right.

proposed in Ref. [40] to engineer a synthetic Turing system is a network of this class, as it is shown in Appendix D 4. Oscillatory Turing filters have less patterning power than stationary Turing filters: Noisy initial conditions or stochastic dynamics combined with oscillations gradually degrade the initial prepattern and evolve to form an oscillating salt-and-pepper pattern of large amplitude. However, if the system follows deterministic dynamics, the amplification of input perturbations with a characteristic wavelength that falls in the flat region of the dispersion relationship is comparable to the amplification of salt-and-pepper patterns. In this instance, oscillatory Turing filters can produce a pattern that results from the oscillatory coupling of several modes, and rich dynamics can ensue.

VI. TOPOLOGY AND ROBUSTNESS

A common criticism about Turing systems is that they are not robust, because small parameter variations impair their patterning potential. This feature is related to what has been referred to as the fine-tuning problem, noting that Turing systems require either unrealistic separation of diffusion scales or unphysical adjustment of kinetic parameters [11]. Generally, it is not known what determines the size of the parameter space of a Turing system. Murray investigated the robustness of several two-node Turing models and found large variations in the size of their Turing space [25], i.e., the combinations of parameters that can result in pattern formation. Several biologically motivated models have shown that the size of the parameter space of Turing systems based on receptor-ligand interaction massively increases when the diffusion of the receptor is restricted to single cells [20,41] or is assumed to be immobile [21,23]. Previously, we made a computational screen to find all minimal Turing networks of three and four nodes with two diffusible species [26]. The calculation of the size of the Turing parameter space revealed a trade-off between stability and instability conditions. More recently, a similar approach was used in Ref. [42] to numerically assess the robustness of two-node and three-node networks. These observations can be partially understood in the framework of our theory. All minimal Turing networks of a given number of nodes can be grouped into a limited number of topological families. A topological family has a unique and minimal distribution of cycles that allows us to build networks that can be stable without diffusion and that can undergo diffusion-driven instabilities.

For example, the 21 nonisomorphic Turing networks of three nodes found in our previous computational screen [26] can be grouped into just seven topological families shown in Fig. 5(a). Similarly, we found 64 nonisomorphic Turing networks of four nodes that can be classified into the 12 topological families that are shown in Sec. VII of the Supplemental Material [37] (together with a conjecture about larger minimal topologies). Crucially, all networks that belong to the same topological family have an identical stability space. Furthermore, the size of the stability space of different topological families varies markedly, as shown in Fig. 5(b). The reason is that the stability space is formed by the intersection of the hypersurfaces defined by the Routh-Hurwitz stability conditions. Importantly, these conditions depend only on the network cycles and ℓ_R-subgraphs that they form. Because of this, and restricting the analysis to systems in which the strength of the interactions between species does not depend on the steady state, the stability space is determined exclusively by the topological family of the network. The Turing space, in turn, is the fraction of the stability space that is compatible with diffusion-driven instabilities and is determined by the diffusion rates. The key variable that determines this fraction is the ratio between the diffusion rates of the nodes that induce the destabilizing module and its complementary nodes. If all nodes diffuse and this ratio tends to 1, the volume of Turing space tends to 0. This is precisely the source of the fine-tuning problem: If realistic

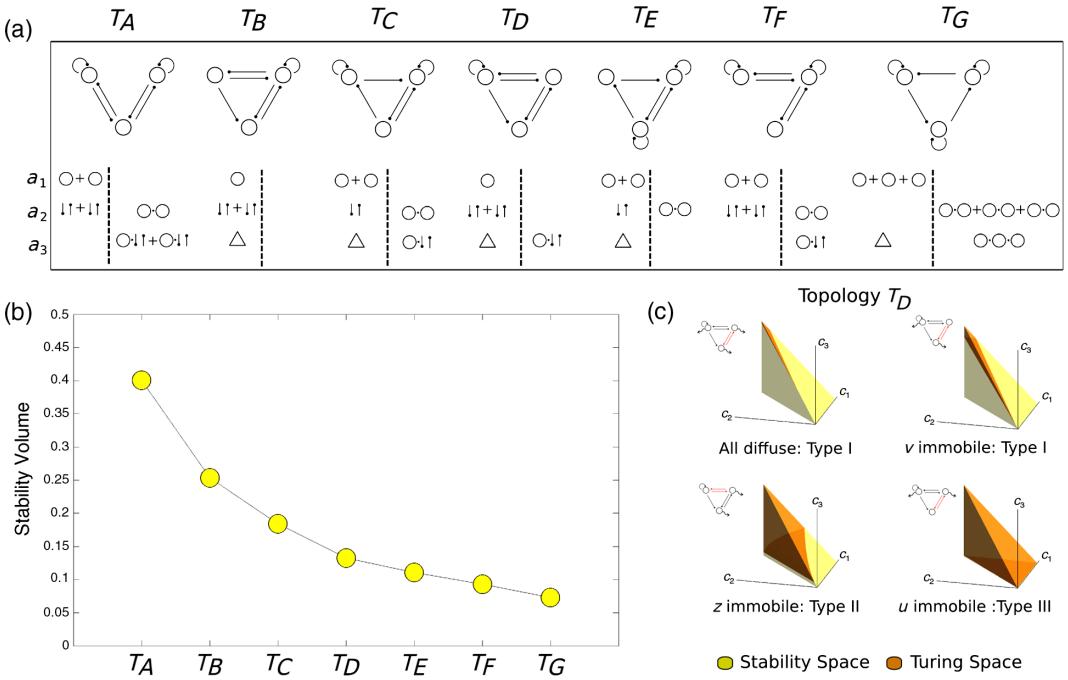

FIG. 5. (a) Seven topological families contain all minimal three-node Turing networks. For each family, the characteristic distribution of cycles and ℓ_R-subgraphs that form $a_k(0)$ is shown at the bottom. (b) Volume of the stability space of the three-node topological families. For all Turing networks within a family, the stability space is the same. (c) Variation of the Turing space for T_D networks when all nodes diffuse (in the top left panel, fine-tuning of kinetic parameters is necessary) or one of the nodes is immobile (for the rest, fine-tuning is not required and $d = 1.5$ in all cases). Volumes of stability and Turing spaces are calculated following the method detailed in Appendix E.

differences in diffusion rates are assumed, the volume of Turing space becomes infinitesimal. The cause of this behavior is then related to the cause of diffusion constraints: It stems from Decartes's rule and the opposite requirements of stability without diffusion and instability with diffusion. These two requirements can be combined in a particularly simple form if the destabilizing module ℓ^{ins} does not overlap with the stabilizing subgraphs of the same size $(\ell_1^{\text{st}}, \ldots, \ell_m^{\text{st}})$:

$$d^{N-k} > \frac{|\ell_1^{\text{st}}| + \ldots + |\ell_m^{\text{st}}|}{|\ell^{\text{ins}}|} > 1, \tag{12}$$

where d is the ratio between the diffusion of nodes complementary to the destabilizing module and the nodes that induce it, and k is the size of the destabilizing module. Note that, as d tends to 1, the space of reaction parameters that can fulfill both inequalities vanishes. However, as demonstrated before, this behavior depends on the assumption that all nodes diffuse. If there are nodes in the destabilizing module that are immobile, the second inequality does not apply, and networks of different types can be obtained. Even if all the nodes that diffuse do so at the same rate, the Turing space does not vanish, as shown in Fig. 5(c) for a particular topological family. Thus, the robustness of a Turing network results from a combination of two factors: (i) the topological family, which determines the volume of the stability space, and (ii) the type given by which nodes are immobile, which determines the Turing space. This illustrates the power of analyzing Turing systems through a topological lens—it demonstrates that the fine-tuning problem is not intrinsic to Turing systems, it reveals its source, and it shows how to bypass it.

VII. TOPOLOGY AND PATTERN PHASES

The original two-node network postulated by Turing can be implemented in two different forms, typically referred to as "activator-inhibitor" and "substrate-depleted" models [43]. The activator-inhibitor network forms a periodic pattern in which the concentrations of the two species are in phase, whereas, in the substrate-depleted network, they are out of phase. Both networks have the same topology, as depicted in Fig. 6: a node with a positive loop and a node with a negative loop connected by negative cycle of length 2, but with the signs of the edges flipped. Thus, the two networks have the same distribution of cycles and cycle signs but differ in the signs of their edges, which leads to the difference in patterns. For both networks, the analytic expression of the conditions for Turing instability and the dispersion relationship are identical, so that the wavelength and speed of growth of the patterns generated are also identical, provided that the kinetic parameters have the same absolute values [44]. The analysis of Turing networks

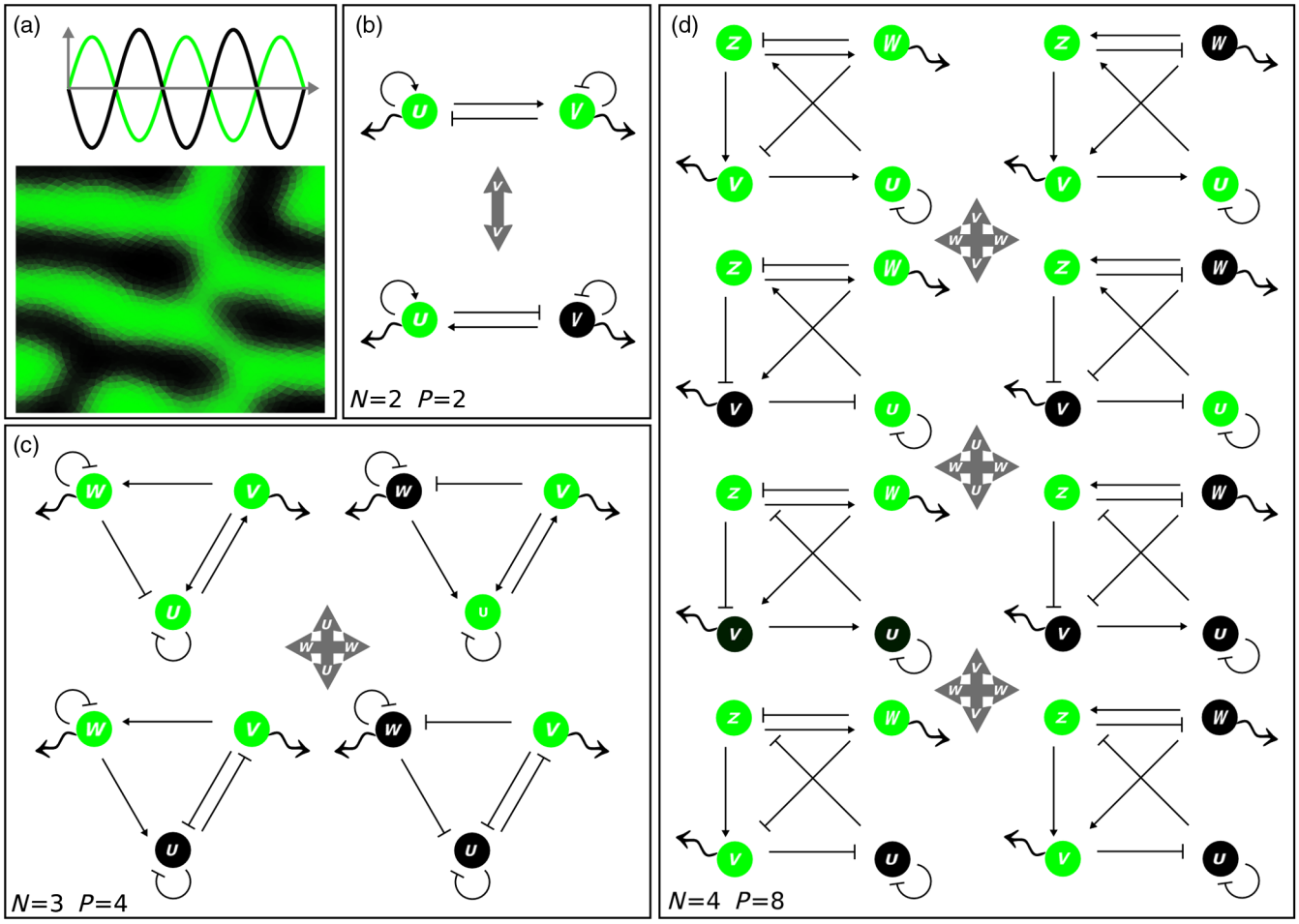

FIG. 6. (a) The concentration of any pair of species in a Turing pattern can be in phase or out of phase. (b) There are two two-node Turing networks, the activator-inhibitor network (top), where the species are in phase, and the substrate-depleted network (bottom), where the species are out of phase. In general, there are 2^{N-1} ways to group N species in two phases of a Turing pattern. An N-node topology allows us to construct 2^{N-1} different Turing networks by switching the signs of the incoming and outgoing edges of one particular node at a time, leaving the cycle signs invariant. Each network makes one of the patterns. Grey cursors indicate that the signs of the edges going in and out of a node have been switched, producing a change in phase. Nodes with the same color are in the same phase. (c),(d) Illustration of this principle for example topologies of $N = 3$ and $N = 4$ nodes, which generate $P = 4$ and $P = 8$ networks and patterns.

through the graph-theoretical lens shows how these properties carry over for networks of any number of nodes and, particularly, how topology governs the pattern phases and which modifications result in the phase-switch of a species.

First, networks that have the same topology and the same distribution of cycle signs are restricted to identical restrictions to requirements for the existence of diffusion-driven instabilities and generate patterns with the same wavelength and growing speed. The reason for this is that the conditions for stability without diffusion and for Turing instability depend exclusively on ℓ-subgraphs and cycles, rather than individual kinetic parameters. Thus, kinetic parameters and diffusion rates are subjected to the same restrictions for the existence of Turing patterns. For the same reason, the dispersion relationship of these networks is identical, so that the dynamics and wavelength of the pattern that they generate are the same.

Second, N species can be grouped in two phases in exactly 2^{N-1} different ways. This is, therefore, the number of different Turing patterns that N species could hypothetically form. For example, a three-node network can form $4 = 2^{3-1}$ patterns: one pattern with all species in phase and three patterns with one of the species being out of phase with the rest. A four-node network can form $8 = 2^{4-1}$ patterns: one with all species in phase, four with one species being out of phase with the rest, and three with a pair of the species out of phase with the other pair. The central finding is that each of these 2^{N-1} patterns is produced by one of the 2^{N-1} Turing networks that share the same topology and cycle signs, but differ in the sign of individual edges. Given a network that produces a pattern with a certain distribution of species amongst the two phases, it is possible to construct a network that produces

the same pattern—but with a single species switched to the other phase—by flipping the signs of all the edges coming in and out of the corresponding node. Note that this transformation leaves invariant the sign of all the cycles passing through the node, including the loops. Applying the same transformation to several nodes at a time, the associated species switch to the opposite phase. There are exactly 2^{N-1} different networks that can be constructed in this way, each generating one of the 2^{N-1} possible Turing patterns. The formal proof in terms of similarity transformations of the Jacobian of the reaction-diffusion equations is given in Sec. V of the Supplemental Material [37]. Intuitively, it can be understood that the effect of switching the signs of the edges going in and out of a node is equivalent to inverting the concentration of this node.

In addition, we find that examination of the topology of a Turing network also allows us to determine the phases of the reactants (if pattern formation occurs in the regime that can be predicted by linear stability analysis). Typically, this is done by calculating numerically the eigenvectors of the linearized system for a particular choice of parameter values. Conversely, the heuristic method that we detail in Appendix F is based on examining the topology and is independent of parameter values, thus providing a more intuitive understanding of Turing dynamics.

VIII. DISCUSSION

In recent years, Turing's theory of pattern formation has received renewed attention because of the increasing evidence of its role in biology, chemistry, and physics. The effects of domain growth [45], complex boundary conditions [46], spatial variation of parameters [47], pattern selection [48], behavior in lattices [49,50], and even centrifugal forces [51] in Turing systems have been studied theoretically. In contrast, the role of the topology underlying a Turing system in shaping its properties has remained largely unexplored. In this paper, we developed a graph-theoretical framework to study this relationship. We find that topology allows us to solve two longstanding questions about Turing systems and to discover a new property.

Firstly, we analyzed the requirement of differential diffusion. For a long time, it was believed that Turing systems were severely restricted because of this requirement, and the only known way to relax this limitation was to add an immobile substrate to trap the self-activating species. This method was discovered serendipitously in the CIMA chemical reaction [17], and the analogous biological principle, known as hindered diffusion [52], biased the search for molecules that could act on a Turing species in development, since the candidate networks were assumed to have to conform to this very specific arrangement. The present theory demonstrates how other arrangements result in greater relaxation and reveals which species must be assumed to be immobile to achieve it. Further, it shows that in larger Turing networks with immobile species, the requirement for differential diffusivity should be the exception, rather than the rule.

Even though relaxation involves necessarily immobile species, this is not an unrealistic limitation. In a biological context, it could be implemented by transcription factors or membrane receptors (which are the majority of proteins involved in gene regulation and do not leave individual cells) playing the role of immobile species and interacting with diffusible ligands (which can cross the cellular membrane and diffuse in the extracellular matrix) playing the role of diffusible species. Likewise, in a chemical reaction, any reactant that is bound or trapped in the medium where the reaction occurs (like starch in the gel of the CIMA reaction [2]) could play the role of an immobile species and does not need to be inert to the rest of the reactants, which affords a design flexibility that so far has not been exploited. Hence, our theory suggests many plausible alternatives for Turing patterns to play a role in biology and chemistry, and it suggests that they could also be more pervasive than previously thought in other areas.

Secondly, we addressed the question of whether Turing systems are intrinsically unrobust, because of the observation that, in most models, unless the kinetic parameters are adjusted with extremely high precision, the patterning power is lost. Our analysis shows that specific topological families stand out for their large stability spaces, which, combined with the method to relax diffusion constraints, results in networks with large Turing spaces. This proves that Turing systems do not require unphysical adjustment kinetic parameters or diffusion rates and can, in fact, be very robust.

Finally, we turned to the investigation of the spatial distribution of the species in a Turing pattern. It is well known that the two classical two-node Turing networks, the activator-inhibitor and the substrate-depleted networks, form patterns with the species in phase and out of phase, respectively [43]. The graph-based analysis reveals the generalization of this property for more complex networks: Examination of the topology of a network suffices to predict the compositions of the two phases of a Turing pattern. Further, we discover that it is possible to modify a network to produce a pattern with any desired combination of species in the same phase. This discovery should be of practical interest to bioengineers, since it opens the door to design synthetic tissues with targeted combinations of genes coexpressed.

Thus, from a theoretical perspective, the present theory provides a unifying view of Turing systems that clarifies poorly understood properties, but also reveals new avenues of inquiry. As an example, in Appendix C, we show how the topological framework greatly facilitates the design and analysis of a Turing system with ten species. Interestingly, preliminary exploration of its behavior suggests that new dynamical phenomena may be intrinsic to Turing systems of a large size.

From a more applied perspective, the present theory should also be of use. In experimental systems, it is easier to obtain reliable information about the topology of a network than precise values of reaction rates or diffusion constants. This is especially true for gene and protein networks in biology, because these parameters are generally estimated from *in vitro* experiments, and yet the real effective values *in vivo* are likely to be quite different. Consequently, a theory that allows us to determine properties of a Turing system from its topology ideally complements quantitative measurements to obtain novel insights into patterning systems and to infer circuits underlying biological patterns.

Finally, the present work could help to answer what is perhaps the most relevant question about Turing systems: Do they actually play an important role in biological development? Strong evidence suggests that this is the case during early patterning of the palate [53], limb [26], hair follicles [54], insect corneae [55], fish [56] and lizard [57] skins, etc. This evidence is, however, not indisputable. There have been many attempts to engineer synthetic networks in a field of cells to produce a Turing pattern of gene expression, but none has succeeded in providing the definitive experimental demonstration [58]. In part, the difficulty stems from the fact that most efforts have followed the designs of classic Turing networks [40]. Here, we provided theoretical tools to widen the repertoire of designs that could be implemented and to analyze their robustness and constraints. This should aid us to finally implement a Turing network in biological cells and prove conclusively that they can, indeed, use Turing patterns to self-organize.

ACKNOWLEDGMENTS

The authors thank Marco Musy and Jim Swoger for useful discussions and Philipp Germann and James Cotterell for revising the manuscript. This research was supported by the ERC advanced grant SIMBIONT (670555) and the Ministerio de Economía y Competitividad (through Centro de Excelencia Severo Ochoa 2013-2017, SEV-2012-0208). X. D. acknowledges support by the ERC-FP7 Grant Swarmorgan (601062). J. S. ackowledges support from ICREA. P. M. and L. M. were supported by ERC Starting Grant QUANTPATTERN (637840).

APPENDIX A: THE REACTION-DIFFUSION GRAPH

The reaction-diffusion graph of a reaction-diffusion system is a weighted digraph associated to the matrix $\mathbf{F^{RD}}(q) = \mathbf{J}^R(r_0) - q^2\mathbf{D}$, obtained from the linear approximation of the reaction-diffusion equations. The definition of the reaction-diffusion graph, denoted as $G[\mathbf{F^{RD}}]$, is based on the definition of the Coates graph of a matrix, whose introduction has been attributed to Coates [35]. Briefly, $G[\mathbf{F^{RD}}]$ is a weighted directed graph of N nodes that has an edge from the jth node to the ith node if the entry $\mathbf{J^R}(r_o)_{ij}$ is nonzero. In addition, for each nonzero entry in $\mathbf{D}$, a special type of edge represented by a wriggled arrow is added to the corresponding diffusible node. A good introduction to the graph-theoretical foundations of this formalism can be found in Brualdi's book [33], and a detailed explanation of its adaptation to the analysis of reaction-diffusion systems was given in Ref. [59]. Similarly, a reaction graph denoted as $G[\mathbf{J^R}]$ can be associated to the Jacobian of the reaction term. Here, we provide a summary of the essential results and examples to illustrate the definitions. Figure 7(a) depicts the reaction-diffusion graph of a minimal four-species Turing system. All species are assumed to diffuse. It has four cycles that are

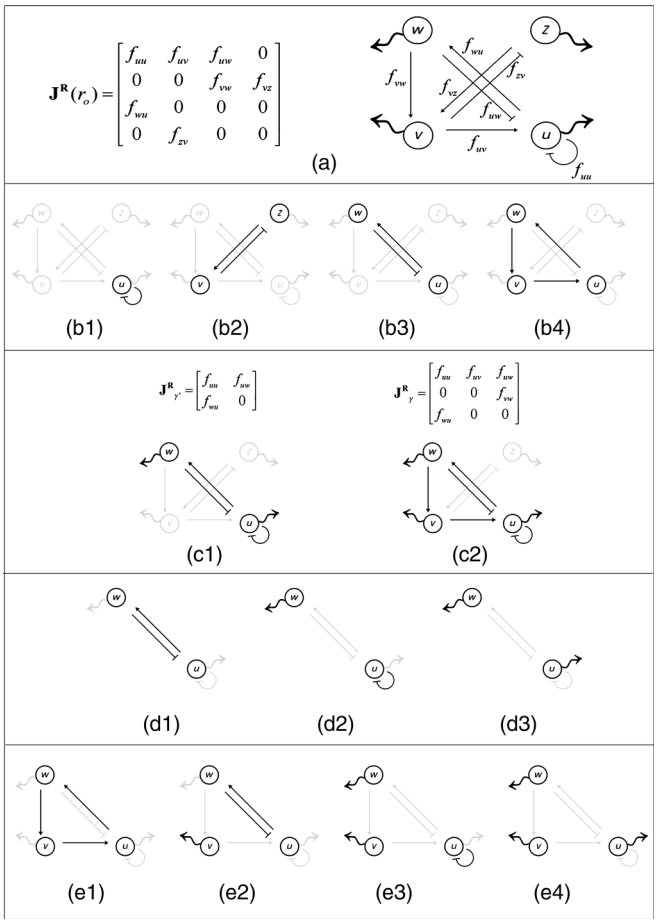

FIG. 7. (a) Jacobian of the reaction term and corresponding reaction-diffusion graph of a four-species Turing system. (b1)–(b4) Four reaction cycles contained in the graph: $\circlearrowleft_u = f_{uu}$, $\underset{vz}{\uparrow\downarrow} = f_{vz}\cdot f_{zv}$, $\underset{uw}{\uparrow\downarrow} = f_{uw}\cdot f_{wu}$, and $\underset{uwv}{\triangle} = f_{wu}\cdot f_{vw}\cdot f_{uv}$. (c1), (c2) Subgraphs induced by $\gamma' = (u, w)$ and by $\gamma = (u, v, w)$, with the corresponding principal submatrices of $\mathbf{J^R}$ shown above. (d1)–(d3) ℓ_R-subgraphs contained in $I_{\gamma=(u,w)}$. (e1)–(e4) ℓ_R-subgraphs contained in $I_{\gamma=(u,v,w)}$. Graph components that do not form part of a subgraph are dimmed.

shown in Fig. 7(b). Using the graph notation introduced in the main text, it is possible to use a single symbol to denote the product of Jacobian entries that form their weight.

Intuitively, the subgraph induced by a subset of nodes is the subgraph formed by these nodes and the edges between them. According to this definition, the subgraph I_{γ_k} induced by the nodes $\gamma_k = (i_1, i_2, \ldots, i_k)$ corresponds to the Coates graph $G[\mathrm{F}^{\mathrm{RD}}_{\gamma_k}]$, where $\mathrm{F}^{\mathrm{RD}}_{\gamma_k}$ is the submatrix formed by row and column indexes in γ_k. In this way, we can establish a one-to-one correspondence between each principal submatrix $\mathrm{F}^{\mathrm{RD}}_{\gamma_k}$ and an induced subgraph I_{γ_k}. Examples of this correspondence for two induced subgraphs of the example network are shown in Fig. 7(c). There are $\binom{N}{k}$ different k-by-k principal submatrices in an N-by-N matrix. The coefficient $a_k(q)$ of the characteristic polynomial $P_q(\lambda)$ is given by the sum of the signed determinants of all the k-by-k principal submatrices [34]:

$$a_k(q) = \sum_{\gamma_k} (-1)^k \det[\mathrm{F}^{\mathrm{RD}}_{\gamma_k}(q)]. \tag{A1}$$

The Coates-Harary formula provides a graphical interpretation of the determinant of a matrix. Precisely, the signed determinant of a k-by-k matrix $\mathrm{F}^{\mathrm{RD}}_{\gamma_k}$ is given by the sum of the weights of all ℓ-subgraphs contained in the induced subgraph I_{γ_k},

$$(-1)^k \det[\mathrm{F}^{\mathrm{RD}}_{\gamma_k}(q)] = \sum_{\ell \subseteq I_{\gamma_k}} w(\ell), \tag{A2}$$

where an ℓ-subgraph contained in I_{γ_k} is a set of nonoverlapping cycles (including the diffusive loops) that span all the nodes in γ_k, and its weight is given by the product of the weights of its cycles and a factor -1 for each of them:

$$w(\ell) = \prod_{c \subseteq \ell} [-w(c)]. \tag{A3}$$

Examples of induced subgraphs of size 2 and 3 in the example network are shown in Fig. 7(c), and the ℓ-subgraphs contained in them are shown in Figs. 7(d) and 7(e).

Introducing Eqs. (A2) and (A3) in Eq. (A1), and splitting the contribution of each induced subgraph in purely reactionlike graphs, mixed and purely diffusive, we can express $a_k(q)$ as

$$a_k(q) = \sum_{I_{\gamma_k}} \Bigg[\sum_{\ell_R \subseteq I_{\gamma_k}} w(\ell_R) + \sum_{\gamma_m \subset \gamma_k}^{m<k} q^{2m} \Bigg(\prod_{j \in \gamma_m} d_j \Bigg) \cdot \Bigg(\sum_{\ell_R \subseteq I_{\gamma_k - \gamma_m}} w(\ell_R) \Bigg) + q^{2k} \prod_{j \in \gamma_k} d_j \Bigg]. \tag{A4}$$

Hence, the coefficients $a_k(q)$ of $P_q(\lambda)$, which determine the stability of the system without diffusion and the existence of diffusion-driven instabilities, can be easily calculated as a sum of all the ℓ-subgraphs of size k. Figure 8 shows the ℓ-subgraphs of size 4 in the example network.

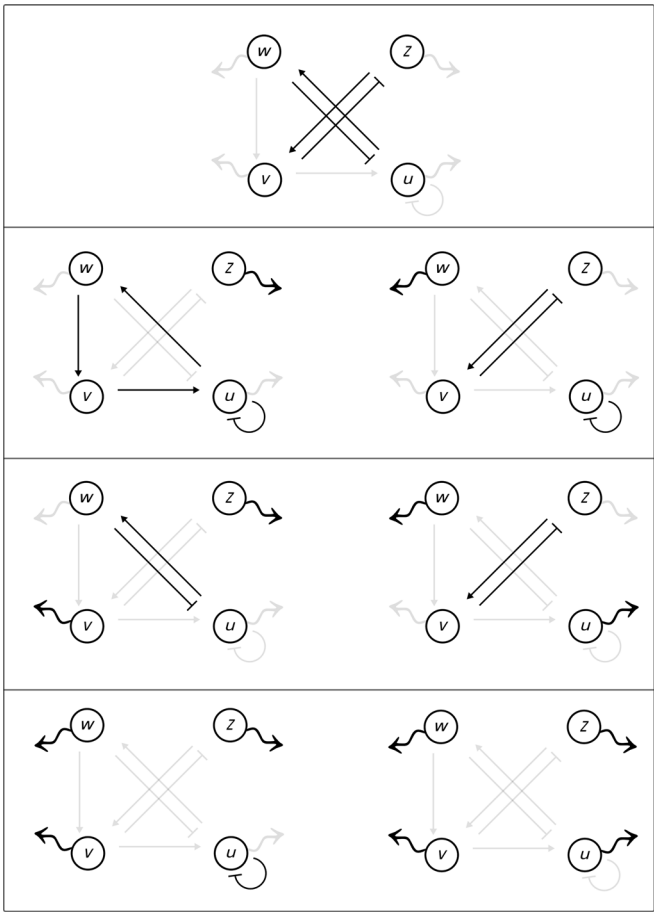

FIG. 8. ℓ-subgraphs of size 4 contained in the network shown in Fig. 7, ordered in rows according to the number of diffusive loops contained.

APPENDIX B: GRAPH NOTATION, CALCULATION OF COEFFICIENTS, AND RELAXATION OF CONSTRAINTS IN A 4N TOPOLOGY

This section demonstrates how to calculate the coefficients of $P_q(\lambda)$ in terms of subgraphs for a four-node topology. The example topology, shown in Fig. 9(a), is particularly interesting because it can be transformed into a type III network by assuming that just one node is immobile. It has four different cycles, listed in Fig. 9(b): a cycle of length 1 (or loop) in node 1; a cycle of length 2 between nodes 1 and 2 and another between 2 and 4; and a cycle of length 3 that joins 2,4, and 3.

A simple recipe to calculate $a_k(q)$ is to go through the subgraphs induced by all possible combinations of k different nodes and sum the ℓ-subgraphs contained in each of them. Thus, trivially, the coefficient $a_1(q)$ is the sum of all cycles of length 1 (including the diffusive loops):

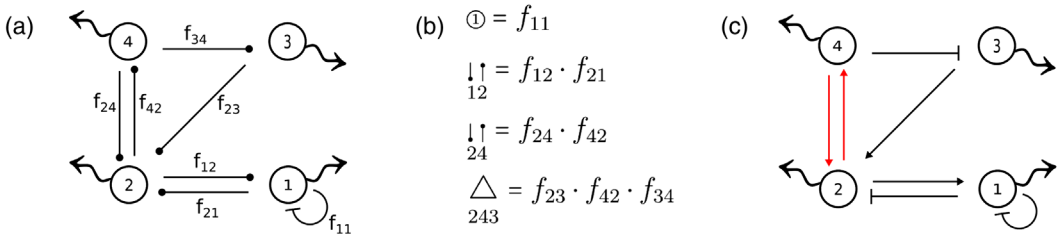

FIG. 9. (a) A minimal four-node topology. (b) Cycles contained in the topology and their weight in terms of the kinetic terms. (c) Turing network based on the example topology. It becomes a type III network just by assuming that node 4 is immobile.

$$a_1(q) = -① + \sum_i q^2 \overset{\uparrow}{\underset{i}{\}}}.$$

Similarly, $a_2(q)$ is the sum of the $\mathscr{C}$-subgraphs contained in all subgraphs induced by two nodes: by nodes 1–2 (the reaction cycle $\underset{12}{\downarrow\uparrow}$, the product of ① with the diffusive loop of node 2, and the product of their diffusive loops); by nodes 2–4 (the reaction cycle $\underset{24}{\downarrow\uparrow}$ and the product of their diffusion loops); by nodes 1–3 and 1–4 (the product of ① with the diffusive loops of the others and the pairs of diffusive loops); and by nodes 2–3 and 3–4 (which only contribute with the products of their diffusive loops). These are

$$a_2(q) = -\underset{12}{\downarrow\uparrow} - \underset{24}{\downarrow\uparrow} -① \sum_{i\neq 1} q^2 \overset{\uparrow}{\underset{i}{\}}} + \sum_{i_1<i_2} q^4 \overset{\uparrow\uparrow}{\underset{i_1 i_2}{\}\}}}.$$

Following the same recipe, the rest of the coefficients can be readily obtained:

$$a_3(q) = -\underset{243}{\triangle} +① \cdot \underset{24}{\downarrow\uparrow} - \underset{12}{\downarrow\uparrow}\left(q^2 \overset{\uparrow}{\underset{3}{\}}} + q^2 \overset{\uparrow}{\underset{4}{\}}}\right) - \underset{24}{\downarrow\uparrow}\left(q^2 \overset{\uparrow}{\underset{1}{\}}} + q^2 \overset{\uparrow}{\underset{3}{\}}}\right)$$
$$-① \sum_{1<i_1<i_2} q^4 \overset{\uparrow\uparrow}{\underset{i_1 i_2}{\}\}}} + \sum_{i_1<i_2<i_3} q^6 \overset{\uparrow\uparrow\uparrow}{\underset{i_1 i_2 i_3}{\}\}\}}},$$

$$a_4(q) = \underset{243}{\triangle} \cdot ① - \underset{243}{\triangle} \cdot q^2 \overset{\uparrow}{\underset{1}{\}}} + ① \cdot \underset{24}{\downarrow\uparrow} \cdot q^2 \overset{\uparrow}{\underset{3}{\}}} - \underset{12}{\downarrow\uparrow} \cdot q^4 \overset{\uparrow\uparrow}{\underset{3\,4}{\}\}}} - \underset{24}{\downarrow\uparrow} \cdot q^4 \overset{\uparrow\uparrow}{\underset{1\,3}{\}\}}} -① \cdot q^6 \overset{\uparrow\uparrow\uparrow}{\underset{2\,34}{\}\}\}}} + q^8 \overset{\uparrow\uparrow\uparrow\uparrow}{\underset{1\,234}{\}\}\}\}}}.$$

Examination of the reaction terms in these coefficients (those without q^2 factors) is informative: It shows the combination of edge signs that are allowable to build a Turing network with the topology of Fig. 9(a). Stability without diffusion requires $a_k(q=0) > 0$, and this imposes strict limitations on which cycle can act as the destabilizing module. From $a_1(0) > 0$, we infer $① < 0$; the loop must be a decay term. Likewise, $a_4(0) > 0$ imposes $\underset{243}{\triangle} < 0$. The condition $a_2(0) > 0$ seems to indicate that any of the cycles of length 2 could be the destabilizing module. This is shown to be false by examining the second Hurwitz determinant $a_1(0)\cdot a_2(0) - a_3(0) = ① \cdot \underset{12}{\downarrow\uparrow} + \underset{243}{\triangle}$, which must also be positive for stability (see Sec. I of the Supplemental Material [37] for details). Hence, we infer that $\underset{12}{\downarrow\uparrow}$ must be negative and that the only possible destabilizing module is then $\underset{24}{\downarrow\uparrow}$. With these limitations, we can choose the signs of the edges in the example topology to build a Turing network. A possible choice is shown in Fig. 9(c). Introducing the cycle signs explicitly in $a_4(q)$ is also informative, since it reveals how to weaken the diffusion constraints:

$$a_4(q) = \underset{243}{\triangle} \cdot ① - q^2 \overset{\uparrow}{\underset{1}{\}}} \cdot \underset{243}{\triangle} + q^2 \overset{\uparrow}{\underset{3}{\}}} \cdot ① \cdot \underset{24}{\updownarrow} - q^4 \overset{\uparrow\uparrow}{\underset{3\,4}{\}\}}} \cdot \underset{12}{\updownarrow} - q^4 \overset{\uparrow\uparrow}{\underset{1\,3}{\}\}}} \cdot \underset{24}{\updownarrow} - q^6 \overset{\uparrow\uparrow\uparrow}{\underset{2\,34}{\}\}\}}} \cdot ① + q^8 \overset{\uparrow\uparrow\uparrow\uparrow}{\underset{1\,234}{\}\}\}\}}}.$$

Indeed, imposing that node 4 is immobile $\left(\overset{\uparrow}{\}}_4 = 0\right)$ transforms the network into a type III because it removes the stabilizing effect of all subgraphs of the same *and* smaller size than the destabilizing module. Hence, the destabilizing module becomes the only contributor to the leading term in $a_4(q)$:

$$a_4(q) = \underset{243}{\triangle} \cdot ① - q^2 \overset{\uparrow}{\underset{1}{\}}} \cdot \underset{243}{\triangle} + q^2 \overset{\uparrow}{\underset{3}{\}}} \cdot ① \cdot \underset{24}{\updownarrow} - q^4 \overset{\uparrow\uparrow}{\underset{1\,3}{\}\}}} \cdot \underset{24}{\updownarrow}.$$

Examination of the topology also allows us to infer the phase occupied by each species without the need to make additional calculations. Following the rule of thumb detailed in Appendix F, we can determine that species 2,4, and 1 are in phase, while

species 3 is out of phase with them. The reason why this topology could be an ideal design to engineer a system that can generate Turing patterns is discussed in Sec. III C of the Supplemental Material [37].

APPENDIX C: DESIGN OF A LARGE TURING NETWORK

The study of Turing systems is generally limited to networks of small size, typically $N = 2$ or $N = 3$ nodes. Here, we show how the present framework facilitates the design of a large network of $N = 10$ nodes. This exercise showcases how the present theory enables finding solutions to a technical challenge and, more importantly, it reveals the existence of unexpected phenomena that may be specific to large Turing systems. There are two main difficulties to overcome in order to design a large Turing network: First, finding a topology that can potentially form a stable reaction network and undergo diffusion-driven instabilities. Second, finding a set of numerical values for the parameters so that the stability and instability conditions are fulfilled. A solution to the first point is guided by the fact that stability requires the coefficients $a_i(0) > 0$ for $i \leq N$, while stationary diffusion-driven instabilities require a destabilizing module of length smaller than N. Topologically, this means that there must be a negative cycle (or stabilizing ℓ-subgraph) of every length up to 10 and a positive cycle of length smaller than 10.

The topology shown in Fig. 10(a) fulfills this criterion. The following strategy was adopted to build it: We draw ten nodes and add a negative loop to n_1 (i.e., node 1); then, we add a cycle of length 2 that connects n_2 to n_1, then a cycle of length 3 that connects n_3 with the previous two, and so on, up to $N - 2 = 8$. The cycle of length $N - 1 = 9$ connecting n_1 to n_9 is set to be the destabilizing cycle and, therefore, positive. The reason to choose a cycle of length $N - 1$ as the destabilizing cycle is to enforce that instabilities associated to $a_{i<N} < 0$ do not occur, because they would result in oscillations and not stationary patterns. Since there must be a stabilizing ℓ-subgraph of the same length as the destabilizing module, we must add an additional negative cycle. In this case, we add an edge that joins n_{10} to n_7 to create an additional cycle of length 4, which, together with the negative cycle of length 5 that joins n_1 to n_5, forms a stabilizing ℓ-subgraph of length 9. Note that there are many other possibilities to achieve the same result (e.g., adding a cycle of length 5 that does not overlap with the existing one of length 4).

Next, we tackle the problem of finding a set of parameter values that fulfill the Turing conditions and resolving the sign of the cycles for which there may be an ambiguity. First, we need to calculate the coefficients $a_i(0)$ and confirm that the network can be stable without diffusion. To ease the notation, we denote the loop at node 1 as c_1; the cycle joining n_1 to n_2 as c_2; the cycle joining n_1, n_2, and n_3 as c_3; and, in this way, up to c_{10} that joins n_1 to n_{10}. The additional cycle of length 4 between $n_7, \ldots, n_{10}$ is denoted by $\bar{c}_4$. With this notation, the coefficients a_i can be expressed compactly as

$$
\begin{aligned}
a_1(0) &= -c_1, & a_2(0) &= -c_2,\\
a_3(0) &= -c_3, & a_4(0) &= -c_4 - \bar{c}_4,\\
a_5(0) &= -c_5 + c_1 \cdot \bar{c}_4, & a_6(0) &= -c_6 + c_2 \cdot \bar{c}_4,\\
a_7(0) &= -c_7 + c_3 \cdot \bar{c}_4, & a_8(0) &= -c_8 + c_4 \cdot \bar{c}_4,\\
a_9(0) &= -c_9 + c_5 \cdot \bar{c}_4, & a_{10}(0) &= -c_{10} + c_6 \cdot \bar{c}_4.
\end{aligned}
$$

Note that, for $i \geq 4$, there is more than one ℓ-subgraph at each order, which may allow different choices of signs for the cycles of the corresponding lengths. Stability conditions are guaranteed if all the Hurwitz determinants are positive (see Sec. I of the Supplemental Material [37] for details). In this example, this involves ten nonlinear algebraic inequalities with up to 10! terms formed by products of ten coefficients $a_k(0)$. Thus, finding a set of parameter values that fulfills these inequalities in the eleven-dimensional space of the cycles is a formidable task. A blind numerical exploration is extremely inefficient, because of the sheer size of the parameter space. In fact, all attempts to find solutions by brute force fail after reasonable computational time, at least if not all the signs of the edges are known. Thus, we propose an efficient method to work around this problem, which is a useful aid to design large Turing networks and also poses the question of robustness in an interesting perspective. The key to the method is simple: From the identity $P_{q=0}(\lambda) = (\lambda - \lambda_1) \cdot \ldots \cdot (\lambda - \lambda_N)$, it follows that $a_i(0) = (-1)^i \sum_{j_1 < \ldots < j_i} (\lambda_{j_1} \cdot \ldots \cdot \lambda_{j_i})$. Hence, instead of searching for values of c_i that result in coefficients $a_i(0)$ that fulfill the Hurwitz conditions, we fix the eigenvalues to arbitrary negative values $\lambda_1 < 0, \lambda_2 < 0, \ldots, \lambda_N < 0$; derive the numerical values of the coefficients $a_i(0)$; and, from them, derive the cycle's weights. Thus, introducing the numerical values of $a_i(\lambda_1, \ldots, \lambda_N)$ in their expressions in terms of cycles, we obtain a much simpler nonlinear system of algebraic equations with c_i as unknowns. For the topology of Fig. 10(a), the system is easily solvable and it has two solutions. In general, the manifold formed by the solutions of this system of equations determines the robustness of the associated Turing network. Hence, it would be interesting to study the relationship between topological properties (such as the number of cycles versus nodes) and the structure of the associated system of algebraic equations obtained in this way. A set of kinetic parameters obtained with this method setting $\lambda_1 = -0.1$, $\lambda_2 = -0.5$, and $\lambda_i = -1$, for $i = 3, \ldots, 10$, is shown in Fig. 10(b). Finally, we need to confirm that the network is capable of undergoing diffusion-driven instability. Again we take advantage of the intuition given by the topological framework and set as diffusible the nodes that are complementary to the

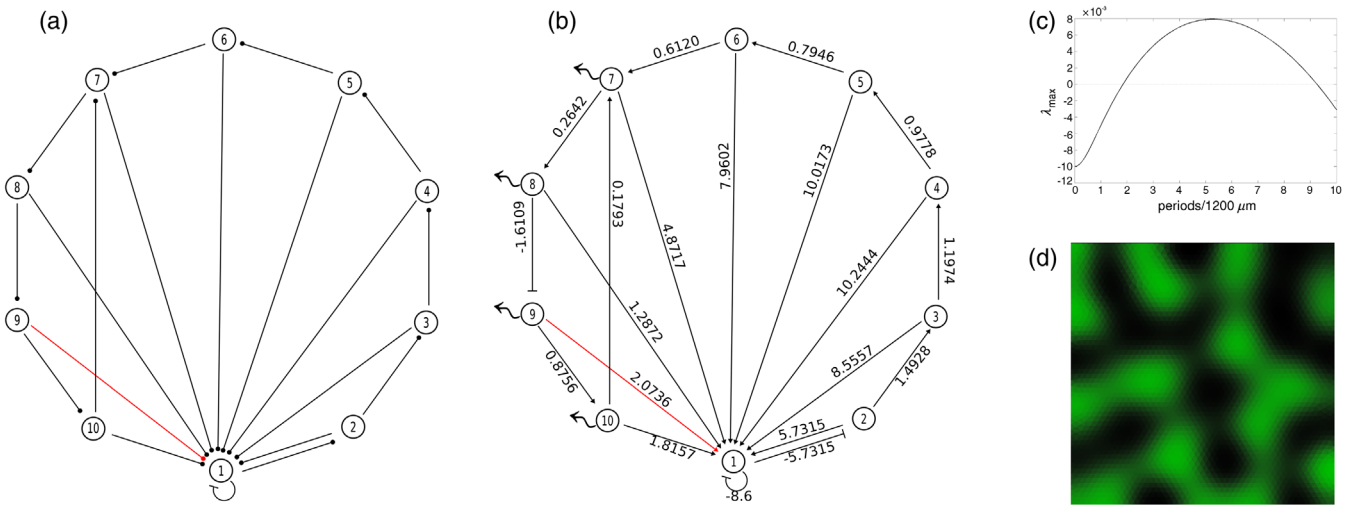

FIG. 10. (a) A ten-node Turing topology. The last edge of the destabilizing cycle is highlighted in red. (b) Distribution of edge signs that make a ten-node Turing network based on the topology in (a). Parameter values are found with a search method tailored for very large systems. (c) Dispersion relationship and (d) numerical simulation of the stationary pattern generated with the parameter values shown in (b).

destabilizing module, in this case just n_{10}. At least one node inside the destabilizing node must be diffusible to avoid a Turing filter. We also impose that n_6 is nondiffusible because it is complementary to $\bar{c}_4 \cdot c_5$. In this way, we avoid its stabilizing effect to compete with the destabilizing module. Indeed, with the choice of diffusible nodes in Fig. 10(b), $a_{10}(q)$ is

$$a_{10}(q) = a_{10}(0) - q^{2}\overset{}{\underset{10}{\wedge}}\cdot c_9 - q^{4}\overset{}{\underset{109}{\wedge\wedge}}\cdot c_8 - q^{6}\overset{}{\underset{1098}{\wedge\wedge\wedge}}\cdot c_7 - q^{8}\overset{}{\underset{10987}{\wedge\wedge\wedge\wedge}}\cdot c_6 .$$

Since the destabilizing module is the only contributor of its size to a_{10}, the network is of type II. Indeed, assigning the same value to all the diffusion rates for $i = 7, \ldots, 10$, the network undergoes diffusion-driven instabilities. The dispersion relationship and the pattern generated are shown in Figs. 10(c) and 10(d). We have also confirmed that the pattern phases can be easily deduced using the rule of thumb: With the choice of signs of Fig. 9(b), it predicts a phase formed by species 1,9,10 and another with species 2 to 8, which we have confirmed numerically. Our exploration of the parameter space of this ten-node network revealed unexpected phenomena, such as stationary patterns with peak doubling, spiral waves, and pulses within stationary patterns. These phenomena occur in specific regions of the Turing space and depend on the saturation terms, so they may occur in regions in which the analysis by linear approximation breaks down. In addition, for the numerical values explored, there are large differences in the amplitudes (the height of the peaks, not the wavelengths) of the patterns made by the different species, caused by the difference in the magnitude of the eigenvectors' components. In conclusion, this suggests that the study of large Turing systems may lead to the discovery of new dynamical behaviors that are intrinsic to systems of their size.

APPENDIX D: ANALYSIS OF TURING MODELS FROM THE LITERATURE

1. The CIMA reaction

The chlorite–iodide–malonic acid (CIMA) reaction was the system in which stationary Turing patterns were first observed [12]. Lengyel and Epstein analyzed a model that correctly describes the temporal behavior of the reaction to investigate the patterning mechanism underlying the reaction [2]. This analysis suggested that starch, introduced as an indicator to visualize the formation of spatial structures, forms a complex with iodine that cannot diffuse in the gel where the reaction occurred. In this way, the effective diffusion of the activator (iodine, I^-) is reduced, producing the difference in diffusion with the inhibitor (chlorite, ClO_2^-) that is required for Turing instabilities. By making a series of reasonable approximations about the underlying chemical processes, the description of the CIMA reaction can be reduced to a three-species reaction-diffusion model [15]. Denoting the concentration of the activator as $[I^-] = u$, the inhibitor $[ClO_2^-] = v$, starch as s_0, and the starch-iodine complex $[SI_3^-] = su$, the Lengyel-Epstein model can be written as

$$\begin{aligned}
\frac{\partial u}{\partial t} &= f(u,v) - k_+ s_o \cdot u + k_- \cdot su + D_u \frac{\partial^2 u}{\partial x^2}, \\
\frac{\partial v}{\partial t} &= g(u,v) + D_v \frac{\partial^2 v}{\partial x^2}, \\
\frac{\partial su}{\partial t} &= k_+ s_o \cdot u - k_- \cdot su.
\end{aligned} \tag{D1}$$

The kinetic constants k_+ and k_- give the rates of formation and dissociation of the starch-iodine complex. Lengyel and Epstein further simplified the analysis by assuming that the formation and dissociation of the complex is very fast.

With this approximation, the concentration of the complex is given by $su = (k_+ \cdot s_0/k_-)u$ because it is in instantaneous equilibrium with the activator u. The CIMA model is then simplified to a set of two reaction-diffusion equations for u and v and, importantly, this transformation introduces a timescale separation between the two species that reflects that the activator is being trapped and released by the starch in the medium. Using realistic values for the parameters in the model, Lengyel and Epstein estimated that, without starch, the diffusion rate of v ought to be ten times faster than that of u to generate Turing instabilities. According to the Stokes-Einstein law, the diffusion of two ions of similar sizes in aqueous solution cannot possibly be that different. However, the introduction of starch reduces the necessary ratio of diffusion rates to a more plausible value of 1.5.

Next, we use our graph-based formalism to analyze the mechanism of relation of diffusion constraints in the CIMA reaction. The analysis does not require the assumption of fast complex formation and, in this respect, is more general. The reaction-diffusion graph associated to the Lengyel-Epstein model of the CIMA reaction given by Eq. (D1) is obtained following the procedure detailed in the main text and shown in Fig. 11.

The activator has two loops that correspond to the self-activation term $\partial f/\partial u$ and the term $k_+ \cdot s_0$ that gives the rate of decrease in the concentration of u through complex formation. In graph notation, this is represented by $\textcircled{u} = \textcircled{u_a} + \textcircled{u_c}$, with the first loop accounting for self-activation and the second for complex formation. In addition, the edges that form the cycle between u and su and their loops are not independent, because the number of iodide molecules is conserved and, therefore, $\underset{u\cdot su}{\Updownarrow} = -\textcircled{u_c} \cdot -\textcircled{su}$. These identities lead to the following simplification of the subgraph induced by u and su:

$$\left(\textcircled{u}\textcircled{su} - \underset{u\cdot su}{\Updownarrow}\right) = \left[\left(\textcircled{u_a} + \textcircled{u_c}\right)\textcircled{su} - \left(-\textcircled{u_c} \cdot -\textcircled{su}\right)\right]$$
$$= \textcircled{u_a}\textcircled{su}\,.$$

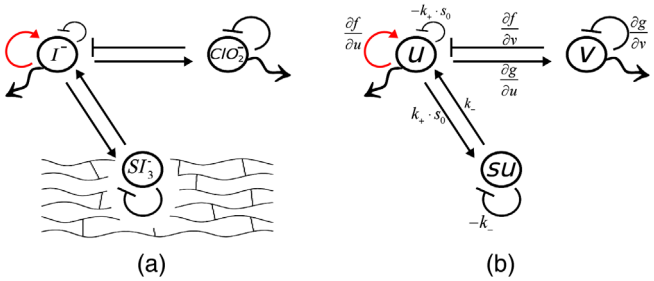

FIG. 11. (a) The CIMA reaction modeled by Lengyel and Epstein [15]. Iodine I^- acts as the activator, chlorite ClO_2^- as the inhibitor, and the starch-iodine complex SI_3^- cannot diffuse because it is trapped by the medium. (b) The reaction-diffusion graph associated to the Lengyel-Epstein model of the CIMA reaction.

In turn, this simplifies the coefficient a_3 of the characteristic polynomial to

$$a_3(q) = a_3(0) + q^2\Big[\textcircled{su}\textcircled{v}\overset{}{\underset{u}{\curvearrowleft}} + \Big(\textcircled{u}\textcircled{su} - \underset{u\cdot su}{\Updownarrow}\Big)\overset{}{\underset{v}{\curvearrowleft}}\Big] - q^4\textcircled{su}\overset{}{\underset{uv}{\curvearrowleft\!\curvearrowleft}}$$
$$= a_3(0) + q^2\Big[\textcircled{v}\overset{}{\underset{u}{\curvearrowleft}} + \textcircled{u_a}\overset{}{\underset{v}{\curvearrowleft}}\Big]\textcircled{su} - q^4\textcircled{su}\overset{}{\underset{uv}{\curvearrowleft\!\curvearrowleft}}\,.$$

Hence, the only term in $a_3(q)$ that can be negative in order to fulfill the necessary condition for stationary Turing patterns is the coefficient of q^2. The form of $a_3(q)$ is characteristic of a type II Turing system according to the diffusion constraints. Indeed, defining $d = \curvearrowleft_v / \curvearrowleft_u$, this condition can be expressed as

$$d > -\frac{\textcircled{v}}{\textcircled{u_a}}\,.$$

Importantly, stability requirements do not force that $\textcircled{u_a}$ is smaller than $\textcircled{v}$, because the network contains other stabilizing loops:

$$a_1(0) = -\left(\textcircled{su} + \textcircled{u_a} + \textcircled{u_c} + \textcircled{v}\right) > 0 \not\Rightarrow \textcircled{u_a} < -\textcircled{v}\,.$$

Hence, the diffusion ratio can be equal to 1 and even smaller, depending on the parameter values of $\textcircled{u_a}$ and $\textcircled{v}$. The explicit form of the constraints for the kinetic parameters can be obtained by examining the rest of the stability conditions $a_i(0) > 0$, but they do not further limit the diffusion ratio of the activator and the inhibitor. Thus, this analysis allows us to easily derive the diffusion constraints of the CIMA reaction and does not require the approximation that complex formation is very fast. Importantly, all network designs based on the CIMA architecture result in a type II Turing system, because of the existence of stabilizing terms involving more diffusion loops. Examples of such networks can be found in Refs. [19–21].

2. Biological models based on the CIMA architecture

In this section, we analyze two Turing models inspired by the CIMA reaction. The first is a recent investigation of the conditions for diffusion-driven instability in the presence of binding immobile substrates by Korvasova *et al.* [19]. This is a purely theoretical study that aimed to weaken the restrictive conditions that apply to diffusion rates and kinetic parameters of two-node Turing networks.

To that end, they analyzed the Lengyel-Epstein model [15] of the CIMA reaction using standard linear stability analysis and algebraic manipulations. They also proposed a four-node generalization of the CIMA model in which two self-activators bind two immobile substrates. The corresponding reaction-diffusion graph is shown in Fig. 12(a).

The principle behind the relaxation of diffusion constraints is the same as in the CIMA reaction. The transient bonds between the activator and substrates do not change the

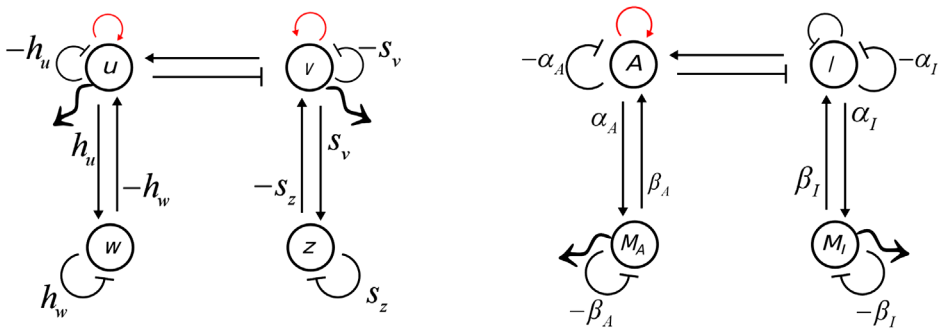

FIG. 12. (a) Network composed of two diffusible self-activators that bind to two immobile substrates [19]. (b) A model of biological patterning based on two morphogens that diffuse in the extracellular space and activate the production of gene products A and I that are confined inside cells [20].

number of molecules. As in the CIMA model, the subgraphs induced by these pairs simplify to $\textcircled{u}\textcircled{w} - \underset{uw}{\updownarrow} = \textcircled{u_a}\textcircled{w}$ and $\textcircled{v}\textcircled{z} - \underset{vz}{\updownarrow} = \textcircled{v_a}\textcircled{z}$, where the loop notation makes explicit the contribution from self-activation and complex formation as in the CIMA reaction. The Turing condition $a_4(q) < 0$ can then be expressed as

$$\begin{aligned} a_4(q) =& a_4(0) + q^2\Big[-\textcircled{z}\Big(\textcircled{w}\textcircled{w} - \underset{uw}{\updownarrow}\Big)\overset{}{\underset{v}{\wr}} - \textcircled{w}\Big(\textcircled{v}\textcircled{z} - \underset{vz}{\updownarrow}\Big)\overset{}{\underset{u}{\wr}}\Big] + q^4 \underset{vu}{\wr\!\wr}\,\textcircled{w}\textcircled{z} \\ =& a_4(0) - q^2\Big(\textcircled{u_a}\overset{}{\underset{v}{\wr}} + \textcircled{v_a}\overset{}{\underset{u}{\wr}}\Big)\,\textcircled{w}\textcircled{z} + q^4 \underset{vu}{\wr\!\wr}\,\textcircled{w}\textcircled{z}. \end{aligned}$$

The existence of two activators introduces an additional relaxation of constraints compared to the original CIMA model: the necessary condition stemming from Decartes's rule of signs is guaranteed because there is a term in $a_4(q)$ formed only by destabilizing terms. However, there is a stabilizing subgraph that contains more diffusive loops and, because of this, the conditions for diffusion-driven instabilities are not independent of the diffusion rates. Still, as in the CIMA reaction, the diffusion rates can be equal, and the network is of type II. The second model to be analyzed was proposed by Rauch and Millonas [20] as a plausible mechanism of biological pattern formation. The model consists of biochemical reactions between gene products that are confined inside cells and, therefore, can be considered nondiffusible and messenger molecules that are secreted by cells and can diffuse between them. The associated reaction graph is shown in Fig. 12(b). Taking advantage of the simplifications that follow from mass conservation as in the previous model, the $a_4(q)$ coefficient can be expressed as

$$a_4(q) = a_4(0) - q^2\Big[\underset{M_A}{\wr}\,\textcircled{M_I}\Big(\textcircled{A_a}\textcircled{I} - \underset{AI}{\updownarrow}\Big) + \underset{M_I}{\wr}\,\textcircled{M_A}\Big(\textcircled{I_a}\textcircled{A} - \underset{AI}{\updownarrow}\Big)\Big] + q^4 \underset{M_AM_I}{\wr}\,\Big(\textcircled{A}\textcircled{I} - \underset{AI}{\updownarrow}\Big).$$

Again, because the nodes A and I are not diffusible, there are stabilizing subgraphs that vanish from the coefficient of degree q^2 in $a_4(q)$. The structure of $a_4(q)$ shows that this network, like CIMA, is also a type II. In this way, the model shows how a realistic physiological model can result in a Turing system that does not require differential diffusivity.

3. Hair follicle formation

A recent work by Klika *et al.* [23] investigated the influence of interactions mediated by immobile receptors in a model of hair-follicle patterning in vertebrate skin. The model was originally proposed by Mou *et al.* [60] and is based in their experimental analysis of the interactions between three key players in hair follicle patterning: a nondiffusing receptor (Edar), a connective tissue growth factor (CTGF), and a bone morphogenetic factor (BMP).

The experimental observations of Mou *et al.* [60] led them to propose the network shown in Fig. 13(a). This network is a Turing filter. We can reach this conclusion without further analysis because the destabilizing module $\textcircled{Edar} > 0$ is nondiffusible. The proof of the generality of this result is given in Sec. IV of the Supplemental Material [37]. Indeed, this can be confirmed by examining the form $a_3(q)$:

$$a_3(q) = a_3(0) + q^2\overset{}{\underset{c}{\wr}}\Big(\textcircled{e}\textcircled{b} - \underset{eb}{\updownarrow}\Big) + q^2\overset{}{\underset{b}{\wr}}\,\textcircled{e}\textcircled{c} - \textcircled{e}\cdot q^4 \underset{bc}{\wr\!\wr}.$$

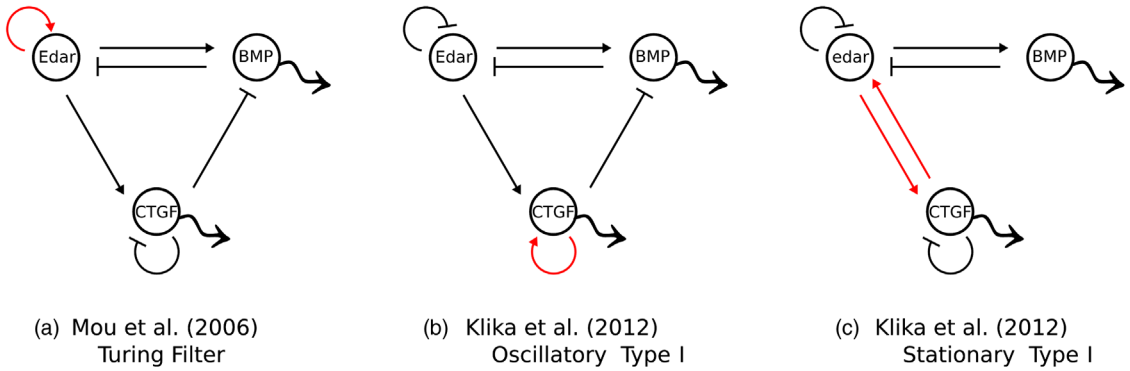

FIG. 13. Three alternative models of hair follicle patterning proposed by (a) Mou *el al.* [60] and (b),(c) Klika *et al.* [23]. They form a Turing filter, an oscillatory Turing network of type I, and a stationary Turing network of type I, respectively.

With the assumed distribution of cycle signs, the condition $a_3(q) < 0$ for Turing instability is fulfilled independently of parameter values for q above a critical value.

Klika *et al.* [23] introduced a series of changes to the model shown in Fig. 13(b) because of theoretical objections. They postulated that Turing systems must be stable for very large wave numbers. If this is not the case, they observed that infinitely small wavelengths would be amplified, in which case the continuum approximation breaks down. Hence, the signs of the loops of Edar and CGTF are inverted, so that the network does not have a nondiffusible self-activator. Laborious algebraic transformations allowed them to prove that the system cannot generate stationary patterns but that it can undergo oscillatory Turing instabilities.

This result is readily recovered using the graph formalism. Stability imposes that $\left(ⓔⓑ - \underset{eb}{\uparrow\!\!\downarrow}\right) > 0$. This means that $a_3(q)$ is formed only by positive terms and, therefore, cannot fulfill the condition $a_3(q) < 0$. However, the coefficient $a_2(q)$ can fulfill $a_2(q) < 0$, the condition for oscillations. This requires $ⓑ > -ⓒ$ and the following constraint on the diffusion ratio:

$$a_2(q) = a_2(0) - q^2 \underset{c}{\uparrow\!\!\!\!\smile}(ⓑ + ⓔ) - q^2 \underset{b}{\uparrow\!\!\!\!\smile}(ⓒ + ⓔ) + q^4 \underset{bc}{\uparrow\!\!\!\!\smile\!\!\!\!\smile} < 0 \Rightarrow \underset{c}{\uparrow\!\!\!\!\smile} / \underset{b}{\uparrow\!\!\!\!\smile} > -\frac{(ⓒ + ⓔ)}{(ⓑ + ⓔ)} > 1\,.$$

This shows that this network is an oscillatory Turing system of type II according to the diffusion constraints. Finally, Klika *et al.* proposed an alternative network for hair-follicle patterning that is shown in Fig. 13(c). The assumption behind this modification is that CTGF does not inhibit the production of BMP directly, but instead inhibits the effects of BMP on Edar. Then, they showed that this network can generate stationary patterns. This result is recovered by examining $a_3(q)$:

$$a_3(q) = a_3(0) + q^2 \underset{b}{\uparrow\!\!\!\!\smile}\left(ⓔⓒ - \underset{eb}{\uparrow\!\!\downarrow}\right) - q^2 \underset{ceb}{\uparrow\!\!\!\!\smile\!\!\downarrow} - ⓔ \cdot q^4 \underset{bc}{\uparrow\!\!\!\!\smile\!\!\!\!\smile} < 0 \Rightarrow \underset{b}{\uparrow\!\!\!\!\smile} / \underset{c}{\uparrow\!\!\!\!\smile} > \frac{\underset{eb}{\uparrow\!\!\downarrow}}{ⓔⓒ - \underset{eb}{\uparrow\!\!\downarrow}} > 1\,,$$

where the second inequality characteristic of type I networks stems from the stability condition $a_2(0) = \left(ⓔⓒ - \underset{eb}{\uparrow\!\!\downarrow}\right) - \underset{eb}{\uparrow\!\!\downarrow} > 0$.

4. A Turing oscillator with a single diffusible molecule

Next, we analyze a design proposed recently as a candidate to engineer a synthetic gene network capable of producing spontaneous diffusion-driven pattern formation in a field of biological cells [40]. The design, shown in Fig. 14(a), is an alternative topology to the classic Turing network: It is based on a three-node unstable oscillatory network quenched by an additional diffusible molecule. Based on the results derived from our theory, it is possible to conclude, without the need to introduce numerical values, that (1) the network can only produce oscillatory patterns and (2) it is a oscillatory Turing filter. The coefficients $a_k(q)$ of the quenched oscillator in terms of subgraphs are

$$a_1(q) = -\sum_{i\le 4} \textcircled{i} + q^2 \overset{\uparrow}{\underset{4}{\}}} = 4 + q^2 \overset{\uparrow}{\underset{4}{\}}},$$

$$a_2(q) = \sum_{i<j\le 4} \textcircled{i}\textcircled{j} - \underset{34}{\uparrow\!\downarrow} - q^2 \overset{\uparrow}{\underset{4}{\}}}(\textcircled{1}+\textcircled{2}+\textcircled{3}) = 6 - \underset{34}{\uparrow\!\downarrow} + 3\cdot q^2 \overset{\uparrow}{\underset{4}{\}}},$$

$$a_3(q) = -\sum_{i<j<k\le 4} \textcircled{i}\cdot\textcircled{j}\cdot\textcircled{k} + (\textcircled{1}+\textcircled{2})\underset{34}{\uparrow\!\downarrow} - \underset{123}{\triangle} + q^2 \overset{\uparrow}{\underset{4}{\}}}(\textcircled{1}\cdot\textcircled{2}+\textcircled{1}\cdot\textcircled{3}+\textcircled{2}\cdot\textcircled{3}) = 4 - 2\cdot\underset{34}{\uparrow\!\downarrow} - \underset{123}{\triangle} + 3\cdot q^4 \overset{\uparrow}{\underset{2}{\}}},$$

$$a_4(q) = \prod_i \textcircled{i} - \textcircled{1}\cdot\textcircled{2}\cdot\underset{34}{\uparrow\!\downarrow} + \underset{123}{\triangle}\cdot\textcircled{4} - q^2 \overset{\uparrow}{\underset{4}{\}}}(\underset{123}{\triangle} + \textcircled{1}\cdot\textcircled{2}\cdot\textcircled{3}) = 1 - \underset{34}{\uparrow\!\downarrow} - \underset{123}{\triangle} + q^2 \overset{\uparrow}{\underset{4}{\}}}(1 - \underset{123}{\triangle}),$$

where the expressions after the second equality result from setting the decay rates of all species at -1 (i.e., $\textcircled{i} = -1$, $\forall i$). Indeed, because of the lack of a positive cycle, all the coefficients are increasing polynomials in q and the conditions of stationary Turing patterns cannot be met. Therefore, the network can only produce oscillatory patterns. The conditions for oscillatory instabilities found in Ref. [40] can be readily derived in terms of the cycles. The first condition imposes that the motive formed by species 1,2, and 3 is unstable: The coefficients of the characteristic polynomial associated to this subnetwork are $\bar{a}_1(0) = -\sum_{i<4} \textcircled{i} = 3$, $\bar{a}_2(0) = \sum_{i<j<4} \textcircled{i}\cdot\textcircled{j} = 3$, and $\bar{a}_3(0) = -\prod_{i<4} \textcircled{i} - \underset{123}{\triangle} = 1 - \underset{123}{\triangle}$. If this subnetwork has to be unstable, the only possibility is that the second Hurwitz determinant is negative: $\bar{a}_1(0)\cdot\bar{a}_2(0) - \bar{a}_3(0) = 8 + \underset{123}{\triangle} < 0$, which leads to $-\underset{123}{\triangle} = b_1\cdot b_2\cdot b_3 > 8$. Conversely, the stability of the full network requires the third Hurwitz to be positive: $a_3(0)\cdot(a_1(0)\cdot a_2(0) - a_3(0)) - a_1^2(0)\cdot a_4(0) = 4(\underset{34}{\downarrow\!\uparrow})^2 - 32\underset{34}{\downarrow\!\uparrow} - (\underset{123}{\triangle})^2 + 64 > 0$, which recovers the second condition $-\underset{34}{\downarrow\!\uparrow} > (-\underset{123}{\triangle} - 8)/2$. Regarding the point that the network is, in fact, an oscillatory Turing filter, it suffices to observe that the subgraph that causes the instability is induced by nondiffusible species. It then follows that, for large wave numbers, the eigenvalues of the full network converge to the (complex) eigenvalues of this subgraph. This can be shown following the proof that characterizes Turing filters (see Sec. IV of the Supplemental Material [37]). The shape of the dispersion relationship shown in Fig. 14(b) and numerical simulations [examples shown in Fig. 14(c)] confirms that this network conforms to the behavior expected from an oscillatory Turing filter.

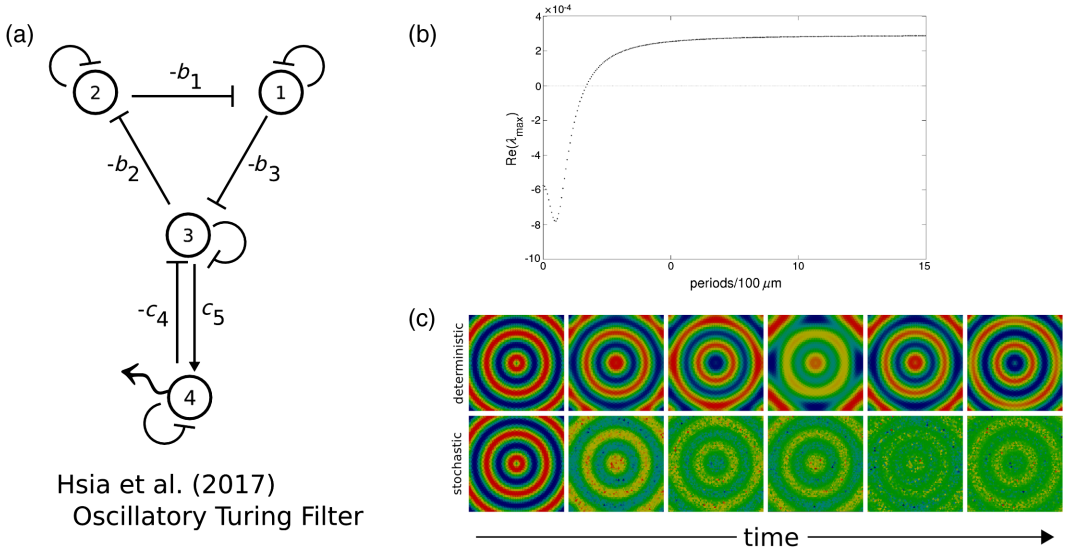

FIG. 14. (a) Design for synthetic genetic Turing network proposed by Hsia *et al.* in Ref. [40]. The system is formed by an unstable oscillatory subnetwork (species 1, 2, and 3) quenched by a single diffusible molecule (species 4). (b) Dispersion relationship characteristic of an oscillatory Turing filter. (c) Oscillatory amplification of a prepattern persists over time under deterministic dynamics (top), but it is degraded and lost after a few periods under stochastic dynamics (bottom).

APPENDIX E: CALCULATION OF THE TURING SPACE

The Turing space of a reaction-diffusion network is formed by the parameter combinations that fulfill the conditions for Turing instability. To assess the robustness of a network, we calculate the volume of the Turing space with fixed values of diffusion rates. Precisely, we set a constant ratio of the diffusion rates of the species in the destabilizing module to the species outside and vary the values of the kinetic parameters. In this way, we can obtain a meaningful comparison of the robustness of two different networks for realistic values of the diffusion rates. Taking advantage of the fact that cycles are the true variables determining the dynamics of a reaction-diffusion system, the volume of the Turing space is calculated in the space formed by the weight of the cycles, rather than the space of individual kinetic parameters. The volume of the Turing space cannot be integrated analytically, because of the complexity of the Turing conditions. Hence, we use Monte Carlo integration to evaluate it numerically. Assuming that kinetic parameters have uniformly distributed random values in [0, 1], the distribution of values of the weight of a cycle formed by k edges is given by the probability density $p(w) = (-1)^{k-1}\log^{k-1}(w)/(k-1)!$, where w is the weight value [61]. If c is the number of cycles in a network, we draw m random values for each cycle from $p(w)$, thus obtaining a grid of m^c points in the space of cycle weights. Let n_s and n_t be the number of points that fulfill the stability and the Turing conditions, respectively. The normalized volumes of the stability space V_s and of the Turing space V_t are then calculated as

$$V_i \approx \frac{n_i}{m^c}, \qquad i = s, t. \tag{E1}$$

For the purpose of visually representing the Turing spaces of the networks, in the main text, we plotted a three-dimensional cross section of them by setting the value of the stabilizing loop to $-1/2$. An interesting feature of this measure is that it permits us to compare the robustness of networks of different sizes, provided that they have the same number of cycles (as is the case for minimal networks of three to five nodes). In addition, this measure of robustness is biologically more meaningful than varying the full set of parameters, since mutations can plausibly produce large changes in the reaction rates between molecules, whereas mutations can hardly produce large changes in the diffusion rates. Alternatively, this measure can be interpreted as the likelihood that a network evolves patterning power through random mutations.

APPENDIX F: RULE OF THUMB TO PREDICT PATTERN PHASES

The topology of a minimal Turing network allows us to predict the phases of the pattern produced. The simple method that we have found is based on examining the cycles of the network. Hence, it does not require us to calculate the eigenvectors of the associated eigenvalue problem. This is particularly advantageous in networks with more than two species, where the analytical solution of the eigenvalue problem is either very cumbersome or, for $N \geq 5$, cannot be found in terms of radicals. Numerical solutions can of course always be found, but they do not provide an intuitive understanding. In addition, in many real systems, the values of the parameters are not known.

The phase of the species in the positive cycle of the destabilizing factor is established first. For any two nodes a and b, the positive cycle connecting them can be divided into two directed paths, one from a to b and another from b to a. Also necessarily, since the cycle is positive, these paths must either be both positive or both negative. In the former case, a and b will be in phase, and in the latter, out of phase. By this simple procedure, the relative phase of every pair of species in the destabilizing module is established.

Next, the phases of the species outside the destabilizing module relative to those inside will be established. Select a node outside the destabilizing module and find a cycle that connects it with a node inside. If the cycle is positive, the phase can be established as before. If the cycle is negative, again, there are just two possibilities for any two nodes a and b in it: either the path from a to b is negative and the path from b to a is positive or the other way around. Let a be the species in the destabilizing module and b the species outside. If the path from a to b is positive, then b is in phase with a. If the path from a to b is negative, then b is out of phase with a. By iteration of this procedure, it is then possible to establish the phase of all the remaining nodes in the network. We have verified that the method allows us to predict correctly the phases of all minimal networks up to five nodes. A few examples are shown in Fig. 15. In nonminimal networks, there may be more than one cycle of the same order connecting the nodes outside the destabilizing module with the nodes that induce it. In this case, there may be an ambiguity if the different connecting cycles have different signs. Then, the cycle chosen to establish the phase of nodes outside the destabilizing module should have the largest weight amongst them. We have tested this method with a few examples of nonminimal networks (including the ten-node network of Appendix C). If the stability conditions impose an invariant hierarchy in the weights of the cycles, then the ambiguity is resolved, and the phases can be inferred just from the topology. However, there may be more complex nonminimal topologies, in which more than one distribution of cycles' signs and relative weights can form a Turing network. In this case, topology is not enough to determine the phases, and the numerical values of the cycles' weight may need to be considered to obtain them. Thus, the general topological rule to determine the phases remains to be found and

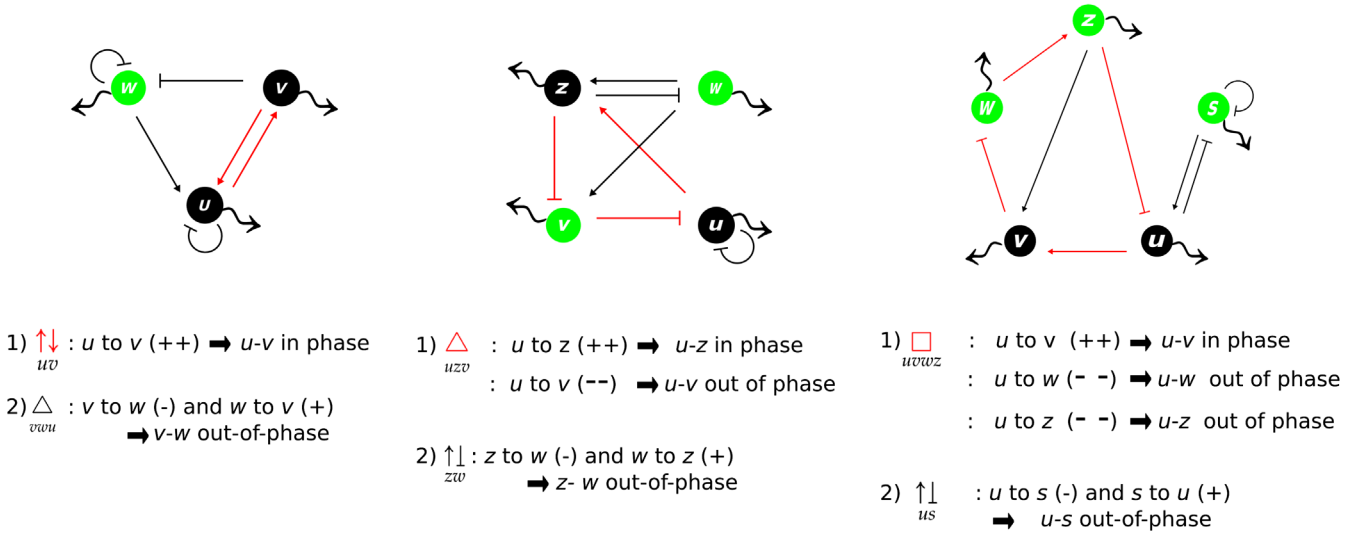

FIG. 15. Examples of the application of the method to establish the phases of the Turing pattern without calculation of the eigenvectors. The positive cycle of the destabilizing module is set in red. Nodes in phase are filled with the same color.

proved rigorously in the general case of nonminimal networks. In addition, it must be emphasized that the topology of the reaction-diffusion graph reflects the linear approximation of the system, and, therefore, the predictions based on the topology hold as long as predictions based on the linear stability analysis hold.

[1] A. M. Turing, *The Chemical Basis of Morphogenesis*, Phil. Trans. R. Soc. B **237**, 37 (1952).

[2] I. Lengyel and I. R. Epstein, *Modeling of Turing Structures in the Chlorite-Iodide-Malonic Acid-Starch Reaction System*, Science **251**, 650 (1991).

[3] L. A. Lugiato and R. Lefever, *Spatial Dissipative Structures in Passive Optical Systems*, Phys. Rev. Lett. **58**, 2209 (1987).

[4] J. Temmyo, R. Notzel, and T. Tamamura, *Semiconductor Nanostructures Formed by the Turing Instability*, Appl. Phys. Lett. **71**, 1086 (1997).

[5] T. Nozakura and S. Ikeuchi, *Formation of Dissipative Structures in Galaxies*, Astrophys. J. **279**, 40 (1984).

[6] L. A. Segel and J. L. Jackson, *Dissipative Structure: An Explanation and an Ecological Example*, J. Theor. Biol. **37**, 545 (1972).

[7] C. A. Klausmeier, *Regular and Irregular Patterns in Semiarid Vegetation*, Science **284**, 1826 (1999).

[8] Y. Shiferaw and A. Karma, *Turing Instability Mediated by Voltage and Calcium Diffusion in Paced Cardiac Cells*, Proc. Natl. Acad. Sci. U.S.A. **103**, 5670 (2006).

[9] M. B. Short, P. J. Brantingham, A. L. Bertozzi, and G. E. Tita, *Dissipation and Displacement of Hotspots in Reaction-Diffusion Models of Crime*, Proc. Natl. Acad. Sci. U.S.A. **107**, 3961 (2010).

[10] J. D. Murray, *Mathematical Biology II* 3rd ed. (Springer, New York, 2003).

[11] T. Butler and N. Goldenfeld, *Fluctuation-Driven Turing Patterns*, Phys. Rev. E **84**, 011112 (2011).

[12] V. Castets, E. Dulos, J. Boissonade, and P. De Kepper, *Experimental Evidence of a Sustained Standing Turing-Type Nonequilibrium Chemical Pattern*, Phys. Rev. Lett. **64**, 2953 (1990).

[13] Q. Ouyang and H. L. Swinney, *Transition from a Uniform State to Hexagonal and Striped Turing Patterns*, Nature (London) **352**, 610 (1991).

[14] K. Agladze, E. Dulos, and P. De Kepper, *Turing Patterns in Confined Gel and Gel-Free Media*, J. Phys. Chem. **96**, 2400 (1992).

[15] I. Lengyel and I. R. Epstein, *A Chemical Approach to Designing Turing Patterns in Reaction-Diffusion Systems*, Proc. Natl. Acad. Sci. U.S.A. **89**, 3977 (1992).

[16] J. Horvath, I. Szalai, and P. De Kepper, *An Experimental Design Method Leading to Chemical Turing Patterns*, Science **324**, 772 (2009).

[17] I. Szalai, J. Horvath, and P. De Kepper, *Contribution to an Effective Design Method for Stationary Reaction-Diffusion Patterns*, Chaos **25**, 064311 (2015).

[18] J. E. Pearson, *Pattern Formation in a $(2+1)$-Species Activator-Inhibitor-Immobilizer System*, Physica (Amsterdam) **188A**, 178 (1992).

[19] K. Korvasova, E. A. Gaffney, P. K. Maini, M. A. Ferreira, and V. Klika, *Investigating the Turing Conditions for Diffusion-Driven Instability in the Presence of a Binding Immobile Substrate*, J. Theor. Biol. **367**, 286 (2015).

[20] E. M. Rauch and M. M. Millonas, *The Role of Trans-Membrane Signal Transduction in Turing-Type Cellular Pattern Formation*, J. Theor. Biol. **226**, 401 (2004).

[21] H. Levine and W. J. Rappel, *Membrane-Bound Turing Patterns*, Phys. Rev. E **72**, 061912 (2005).

[22] D. E. Strier and S. P. Dawson, *Turing Patterns inside Cells*, PLoS One **2**, e1053 (2007).

[23] V. Klika, R. E. Baker, D. Headon, and E. A Gaffney, *The Influence of Receptor-Mediated Interactions on*

Reaction-Diffusion Mechanisms of Cellular Self-Organisation, Bull. Math. Biol. **74**, 935 (2012).

[24] T. C. Lacalli and L. G. Harrison, *Turing's Conditions and the Analysis of Morphogenetic Models*, J. Theor. Biol. **76**, 419 (1979).

[25] J. D. Murray, *Parameter Space for Turing Instability in Reaction Diffusion Mechanisms: A Comparison of Models*, J. Theor. Biol. **98**, 143 (1982).

[26] L. Marcon, X. Diego, J. Sharpe, and P. Müller, *High-Throughput Mathematical Analysis Identifies Turing Networks for Patterning with Equally Diffusing Signals*, eLife **5**, e14022 (2016).

[27] R. G. Casten and C. J. Holland, *Stability Properties of Solutions to Systems of Reaction-diffusion Equations*, SIAM J. Appl. Math. **33**, 353 (1977).

[28] F. R. Gantmacher, *Applications of the Theory of Matrices* (Interscience Publishers, New York, 1959).

[29] M. Mincheva and M. R. Roussel, *Graph-Theoretic Methods for the Analysis of Chemical and Biochemical Networks. I. Multistability and Oscillations in Ordinary Differential Equation Models*, J. Math. Biol. **55**, 61 (2007).

[30] B. L. Clarke, *Graph Theoretic Approach to the Stability Analysis of Steady State Chemical Reaction Networks*, J. Chem. Phys. **60**, 1481 (1974).

[31] B. L. Clarke and W. Jiang, *Method for Deriving Hopf and Saddle-Node Bifurcation Hypersurfaces and Application to a Model of the Belousov-Zhabotinskii System*, J. Chem. Phys. **99**, 4464 (1993).

[32] M. Mincheva and M. R. Roussel, *A Graph-Theoretic Method for Detecting Potential Turing Bifurcations*, J. Chem. Phys. **125**, 204102 (2006).

[33] R. A. Brualdi and D. Cvetkovic, *A Combinatorial Approach to Matrix Theory and Its Applications* (Chapman and Hall/CRC, London, 2008).

[34] R. A. Horn and C. R. Johnson, *Matrix Analysis* (Cambridge University Press, Cambridge, England, 1990).

[35] C. Coates, *Flow-Graph Solutions of Linear Algebraic Equations*, IRE Transactions on Circuit Theory **6**, 170 (1959).

[36] F. Harary, *The Determinant of the Adjacency Matrix of a Graph*, SIAM Rev. **4**, 202 (1962).

[37] See Supplemental Material at http://link.aps.org/supplemental/10.1103/PhysRevX.8.021071 for mathematical proofs of results, examples of the relaxation of diffusion constraints and a conjecture about minimal Turing networks.

[38] M. Mincheva and G. Craciun, *Multigraph Conditions for Multistability, Oscillations and Pattern Formation in Biochemical Reaction Networks*, Proc. IEEE **96**, 1281 (2008).

[39] D. J. Struik, *A Source Book in Mathematics, 1200-1800* (Princeton University Press, Princeton, NJ, 2014).

[40] J. Hsia, W. J. Holtz, D. C. Huang, M. Arcak, and M. M. Maharbiz, *A Feedback Quenched Oscillator Produces Turing Patterning with One Diffuser*, PLoS Comput. Biol. **8**, e1002331 (2012).

[41] T. Kurics, D. Menshykau, and D. Iber, *Feedback, Receptor Clustering, and Receptor Restriction to Single Cells Yield Large Turing Spaces for Ligand-Receptor-Based Turing Models*, Phys. Rev. E **90**, 022716 (2014).

[42] M. M. Zheng, B. Shao, and Q. Ouyang, *Identifying Network Topologies That Can Generate Turing Pattern*, J. Theor. Biol. **408**, 88 (2016).

[43] A. Gierer and H. Meinhardt, *A Theory of Biological Pattern Formation*, Kybernetic **12**, 30 (1972).

[44] T. Miura and P. K. Maini, *Speed of Pattern Appearance in Reaction-Diffusion Models: Implications in the Pattern Formation of Limb Bud Mesenchyme Cells*, Bull. Math. Biol. **66**, 627 (2004).

[45] E. J. Crampin, E. A. Gaffney, and P. K. Maini, *Reaction and Diffusion on Growing Domains: Scenarios for Robust Pattern Formation*, Bull. Math. Biol. **61**, 1093 (1999).

[46] R. Dillon, P. K. Maini, and H. G. Othmer, *Pattern Formation in Generalized Turing Systems*, J. Math. Biol. **32**, 345 (1994).

[47] T. W. Hiscock and S. G. Megason, *Orientation of Turing-Like Patterns by Morphogen Gradients and Tissue Anisotropies*, Cell Systems **1**, 408 (2015).

[48] B. Ermentrout, *Stripes or Spots? Nonlinear Effects in Bifurcation of Reaction-Diffusion Equations on the Square*, Proc. R. Soc. A **434**, 413 (1991).

[49] H. G. Othmer and L. E. Scriven, *Instability and Dynamic Pattern in Cellular Networks*, J. Theor. Biol. **32**, 507 (1971).

[50] H. Nakao and A. S. Mikhailov, *Turing Patterns in Network-Organized Activator-Inhibitor Systems*, Nat. Phys. **6**, 544 (2010).

[51] J. Guiu-Souto and A. P. Munuzuri, *Influence of Oscillatory Centrifugal Forces on the Mechanism of Turing Pattern Formation*, Phys. Rev. E **91**, 012917 (2015).

[52] P. Müller, K. W. Rogers, R. Y. Shuizi, M. Brand, and A. F. Schier, *Morphogen Transport*, Development (Cambridge, U.K.) **140**, 1621 (2013).

[53] A. D. Economou, A. Ohazama, T. Porntaveetus, P. T. Sharpe, S. Kondo, M. A. Basson, A. Gritli-Linde, M. T. Cobourne, and J. B. Green, *Periodic Stripe Formation by a Turing Mechanism Operating at Growth Zones in the Mammalian Palate*, Nat. Genet. **44**, 348 (2012).

[54] S. Sick, S. Reinker, J. Timmer, and T. Schlake, *WNT and DKK Determine Hair Follicle Spacing through a Reaction-Diffusion Mechanism*, Science **314**, 1447 (2006).

[55] A. Blagodatski, A. Sergeev, M. Kryuchkov, Yuliya Lopatina, and Vladimir L. Katanaev, *Diverse Set of Turing Nanopatterns Coat Corneae across Insect Lineages*, Proc. Natl. Acad. Sci. U.S.A. **112**, 10750 (2015).

[56] A. Nakamasu, G. Takahashi, A. Kanbe, and S. Kondo, *Interactions between Zebrafish Pigment Cells Responsible for the Generation of Turing Patterns*, Proc. Natl. Acad. Sci. U.S.A. **106**, 8429 (2009).

[57] L. Manukyan, S. A. Montandon, A. Fofonjka, S. Smirnov, and M. C. Milinkovitch, *A Living Mesoscopic Cellular Automaton Made of Skin Scales*, Nature (London) **544**, 173 (2017).

[58] N. S. Scholes and M. Isalan, *A Three-Step Framework for Programming Pattern Formation*, Curr. Opin. Chem. Biol. **40**, 1 (2017).

[59] X. Diego, *On the Theory of Cell Migration: Durotaxis and Chemotaxis*, Ph.D. thesis, Universitat Politècnica de Catalunya, 2013.

[60] C. Mou, B. Jackson, P. Schneider, P. A. Overbeek, and D. J. Headon, *Generation of the Primary Hair Follicle Pattern*, Proc. Natl. Acad. Sci. U.S.A. **103**, 9075 (2006).

[61] M. D. Springer, *Probability and Statistics Series* (Wiley, New York, 1979).